

## Tropical Thermostats and Low Cloud Cover

R. L. MILLER

*Department of Applied Physics, Columbia University, New York, New York*

(Manuscript received 12 December 1995, in final form 6 June 1996)

### ABSTRACT

The ability of subtropical stratus low cloud cover to moderate or amplify the tropical response to climate forcing such as increased CO<sub>2</sub> is considered. Cloud radiative forcing over the subtropics is parameterized using an empirical relation between stratus cloud cover and the difference in potential temperature between 700 mb (a level that is above the trade inversion) and the surface. This relation includes the empirical negative correlation between SST and low cloud cover and is potentially a positive feedback to climate forcing.

Since potential temperature above the trade inversion varies in unison across the Tropics as a result of the large-scale circulation and because moist convection relates tropospheric temperature within the convecting region to variations in surface temperature and moisture, the subtropical potential temperature at 700 mb depends upon surface conditions within the convecting region. As a result, subtropical stratus cloud cover and the associated feedback depend upon the entire tropical climate and not just the underlying SST.

A simple tropical model is constructed, consisting of separate budgets of dry static energy and moisture for the convecting region (referred to as the "warm" pool) and the subtropical descending region (the "cold" pool). The cold pool is the location of stratus low clouds in the model. Dynamics is implicitly included through the assumption that temperature above the boundary layer is horizontally uniform as a result of the large-scale circulation. The tropopause and warm pool surface are shown to be connected by a moist adiabat in the limit of vanishingly narrow convective updrafts.

Stratus low cloud cover is found to be a negative feedback, increasing in response to doubled CO<sub>2</sub> and reducing the tropically averaged warming in comparison to the warming with low cloud cover held fixed. Increased low cloud cover is shown to result from the increased difference in surface temperature between the warm and cold pools, and the increased low-level static stability over the warm pool, equal to the increase in potential temperature along the moist adiabat originating in the warm pool mixed layer.

### 1. Introduction

The warming predicted by GCMs in response to increasing CO<sub>2</sub> is smallest in the Tropics (e.g., Manabe and Stouffer 1993). Tropical temperatures were also relatively unchanged during past climates such as that of the Cretaceous, when the globally averaged temperature was several degrees warmer (e.g., Budyko and Izrael 1991).

Several feedbacks, or "thermostats," have been proposed to account for the climate stability of tropical convecting regions or the Tropics as a whole, involving, for example, cirrus clouds associated with deep convection (Ramanathan and Collins 1991), upper-tropospheric moisture (Sun and Lindzen 1993b), lateral redistribution of energy by direct circulations (Wallace 1992; Pierrehumbert 1995), surface evaporation (Hartmann and Michelsen 1993), and equatorial ocean dynamics (Dijkstra and Neelin 1995; Clement et al. 1996; Sun and Liu 1996; Seager and Murtugudde 1997).

Here we consider whether the tropical climate is stabilized by subtropical low cloud cover.

Clouds have offsetting effects upon the net radiation passing through the top of the atmosphere. While shielding the earth from solar radiation, they also absorb long-wave radiation emitted by the planet, contributing to the greenhouse effect. High clouds are most efficient at trapping radiation because they emit at temperatures that are relatively cold compared to the earth's surface. The effects of high clouds associated with tropical deep convection upon the incoming solar and outgoing longwave radiation are almost completely offset in the present climate (Ramanathan et al. 1989; Hartmann et al. 1992; Kiehl 1994) so that the net radiative flux at the top of the atmosphere is hardly changed by the presence of these clouds. In contrast, low clouds emit at a temperature closer to that of the surface so that their greenhouse effect is relatively small. On the whole, low clouds act to cool the planet, and regions of strong cloud forcing generally coincide with extensive low cloud cover (Klein and Hartmann 1993).

In this study, we shall focus upon the optically thick low clouds, referred to as "stratus" by the International Satellite Cloud Climatology Project (ISCCP) (Rossow

---

*Corresponding author address:* Dr. R. L. Miller, Goddard Institute for Space Studies, 2880 Broadway, New York, NY 10025.  
E-mail: rlm15@columbia.edu

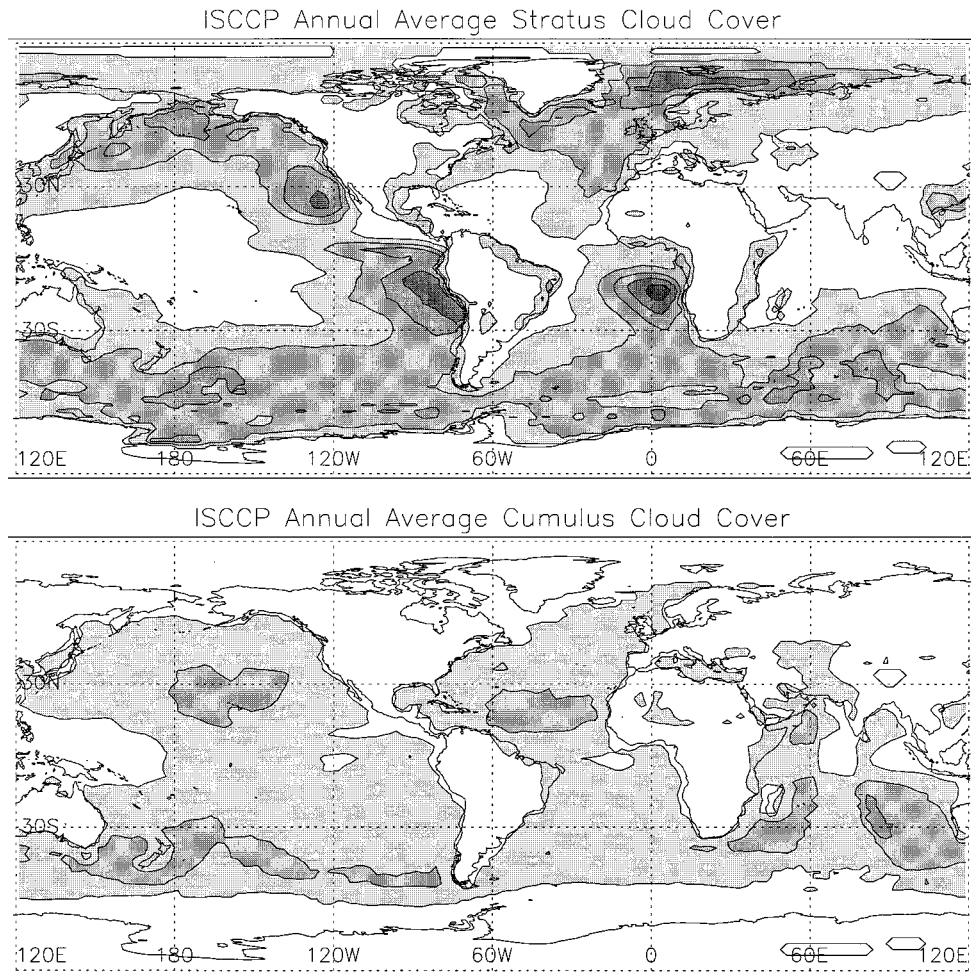


FIG. 1. Annual average of (a) stratus and (b) cumulus low cloud cover for July 1983 to June 1991 as determined by ISCCP. The two cloud types have cloud-top pressures greater than 680 mb and are distinguished by visible optical thickness with stratus clouds corresponding to optical thicknesses greater than 3.6. White regions correspond to cloud cover between zero and 10%, with progressively darker shades corresponding to increases of 10%.

and Schiffer 1991). The radiative forcing associated with these clouds and their relation to the large-scale circulation has been studied by Klein and Hartmann (1993). The annual-mean cloud cover of low stratus clouds as determined by ISCCP is shown in Fig. 1a. Cloud cover is largest in the eastern subtropical oceans, off the coast of Africa and the Americas. Low stratus clouds are also prominent over midlatitude oceans, such as the North Pacific and North Atlantic, along with the circumpolar region in the Southern Hemisphere. In contrast to stratus are the optically thin low clouds, designated by ISCCP as “cumulus.” As shown in Fig. 1b, the region of largest cumulus cloud cover in the Tropics is downwind of the subtropical stratus decks. It is important to note that stratus and cumulus clouds are distinguished by ISCCP based upon visible optical thickness and not cloud morphology. What meteorologists would traditionally regard as a mixture of stratocumulus

and cumulus may comprise a stratus region according to ISCCP. Since stratus and cumulus clouds occur along the same trade wind trajectories (Klein et al. 1995), their variations are presumably correlated, although whether this correlation is positive or negative is at the moment unclear. In this study, we will focus upon the optically thicker stratus low clouds that are observed over the eastern subtropical oceans and estimate their ability to modulate climate change.

The net top-of-the-atmosphere (TOA) forcing by low clouds corresponds to a cooling between 10 and 15  $W m^{-2}$ , when averaged over the Tropics (Hartmann et al. 1992). In comparison, cooling of the Tropics by midlatitude eddies and ocean transport is over 40  $W m^{-2}$  [calculated using the observed poleward export of  $11 \times 10^{15} W$  (Peixoto and Oort 1992)]. In the present-day climate, low clouds do little to cool the Tropics compared to exports to midlatitudes.

However, low clouds may present a significant feedback to climate forcing. A one-percent change in ISCCP stratus low cloud cover corresponds to a change of roughly  $1 \text{ W m}^{-2}$  in ERBE TOA cloud forcing (Klein and Hartmann 1993). For comparison, the TOA radiative perturbation associated with doubled  $\text{CO}_2$  is  $4 \text{ W m}^{-2}$ , leading several authors to suggest that moderate changes in low cloud cover can significantly amplify or else offset the warming associated with increasing  $\text{CO}_2$  (e.g., Randall et al. 1984). Based upon the observed correlation between decreasing low cloud cover and increasing SST, Hanson (1991) and Oreopoulos and Davies (1993) have suggested that low clouds represent a positive feedback to climate perturbations. However, for stratus low clouds, this correlation is only one aspect of a more general relationship between cloud cover and the stability of the lower atmosphere (Klein and Hartmann 1993), which only partly reflects variations in SST. Thus, whether stratus low clouds amplify or moderate the tropical response to climate perturbations depends upon changes in the low-level static stability rather than SST alone.

This leads to the question of what determines low-level static stability in the subtropics, a region of extensive low cloud cover. Static stability, as defined by Klein and Hartmann (1993), consists of the difference between potential temperature at a level above the trade inversion (700 mb in their study) and potential temperature at the surface (essentially equal to SST). Within the subtropical Pacific, temperature variations above the trade inversion and at the surface are uncorrelated (Klein et al. 1995). Variations in potential temperature above the inversion are correlated instead with temperature changes at the same level across the entire Tropics (Sun and Oort 1995). This is a result of the large-scale circulation, where air detains from convective clusters in the deep Tropics and descends toward the trade inversion. Angular momentum is conserved by the zonally averaged component of this circulation, and this constraint together with thermal wind balance results in small horizontal temperature differences across the Tropics (Schneider 1977). Because the vertical profile of temperature in the deep Tropics is related to surface conditions by moist convection (e.g., Betts 1982; Xu and Emanuel 1989; Raymond 1994), potential temperature above the trade inversion is related to the surface conditions of the convecting region. Consequently, low-level static stability in the subtropics, and thus subtropical low cloud cover, depends not only upon the underlying SST, but upon the entire tropical circulation, including the surface conditions in distant convecting regions.

In this article, we construct a simple model of the tropical atmosphere in order to estimate how low-level static stability and stratus cloud cover in the subtropics vary in response to climate forcing. Our model is an extension of the simple one-dimensional thermodynamic models of Sarachik (1978) and Betts and Ridgway

(1989), although our model, like that of Pierrehumbert (1995), allows the climate state of the convecting region and subtropics to vary separately. The model is intended to highlight the feedback due to stratus low cloud cover, and for simplicity, certain feedbacks are omitted. For example, only stratus cloud cover is allowed to change, even though changes in stratus optical thickness may also be important to the climate response to increased  $\text{CO}_2$  (e.g., Tselioudis et al. 1992; Oreopoulos and Davies 1993). In addition, radiative forcing by high clouds is held constant. While high cloud forcing at the TOA is near zero in the current climate (Kiehl 1994) and is a weak function of the underlying SST during ENSO cycles (Ramanathan and Collins 1991), high clouds can substantially change the radiative divergence within the atmospheric column, which in turn affects the strength of the circulation. While our model is incomplete, it is of interest as an estimate of the climate feedback due to subtropical stratus cloud cover alone, especially since it allows the effect of a parameterization similar to that used in many GCMs (e.g., Philander et al. 1996; Slingo 1980; 1987) to be examined in a relatively simple setting. When considered only as a function of local SST, low cloud cover is a positive feedback to climate forcing. This model is intended to relate variations of stratus low cloud cover more generally to the low-level static stability, which requires consideration of the entire tropical circulation.

Our model is described in the next section. It is essentially an elaboration of the model of Pierrehumbert (1995), including a more precise calculation of the radiative fluxes and estimation of the role of clouds. In addition we show that the thermodynamic properties at the surface of the convecting region and the tropopause are linked by a moist adiabat. In section 3, we attempt to reproduce the present-day tropical climate by applying the observed ERBE cloud forcing to the model. In section 4, low cloud cover is allowed to vary in response to perturbations in the tropical climate forced by doubling  $\text{CO}_2$ . The purpose is to estimate whether changes in low cloud cover amplify or moderate the warming of the Tropics. It is found that despite an increase in subtropical SST, low-level static stability increases so that stratus low cloud covers act as a negative feedback, moderating the tropical response to anthropogenic forcing. Our conclusions are given in section 5, where we suggest how other feedbacks can be incorporated into the model.

## 2. Model description

### a. A three-box model

In this section, we construct a model of the tropical climate, following Sarachik (1978), Betts and Ridgway (1989), and Pierrehumbert (1995). (In this article, the "Tropics" refers to the region roughly between  $30^\circ\text{S}$  and  $30^\circ\text{N}$ —essentially the domain of the Hadley cir-

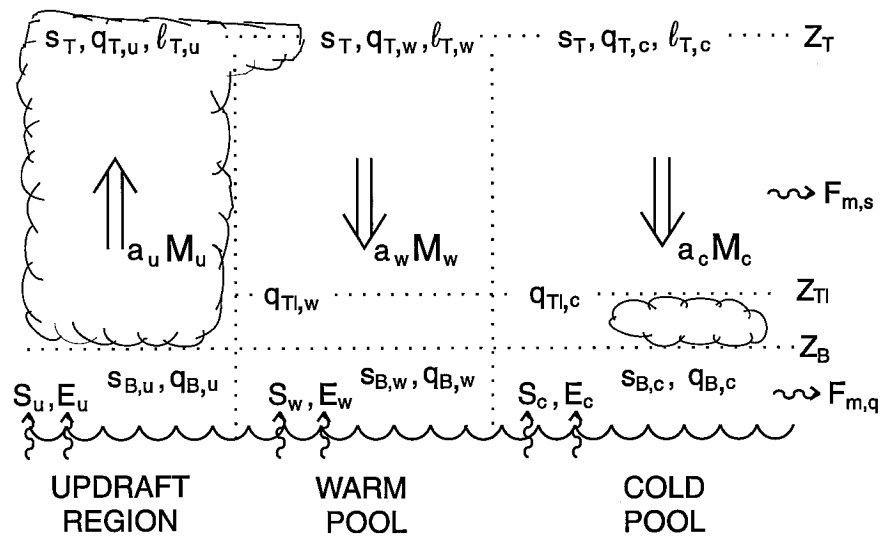


FIG. 2. A schematic of a simple model of the Tropics. Air detrain from the convective updraft at the tropopause  $z_T$ , descends through the trade inversion at  $z_{Ti}$ , and returns to the updraft within the mixed layer of thickness  $z_B$  equal to the lifting condensation level. At the tropopause, there is a mass flux  $a_u M_u$  from the updraft to the warm pool and a flux  $a_c M_c$  from the warm pool to the cold pool with equal and opposite flow below within the mixed layer.

ulation—and thus includes the subtropics in addition to the deep Tropics.) The model is intended to allow subtropical stratus low cloud cover to respond to rising concentrations of  $\text{CO}_2$ , within the context of the entire tropical circulation. Variations in stratus low clouds are empirically related to low-level static stability (Klein and Hartmann 1993), here defined as the difference in potential temperature measured at 700 mb (just above the trade inversion) and at the surface. Potential temperature can vary independently at these two levels since above the trade inversion temperature varies on a tropic-wide scale in response to variations in deep convection (Sun and Oort 1995), whereas below, local boundary layer processes are important.

The model consists of an “updraft” region comprising convective towers, a “warm pool” in which convective towers are embedded, and a “cold pool” within which stratus low clouds form. The three regions are linked dynamically by air that detrain at the top of the updraft and descends over the warm and cold pools before rejoining the surface flow into the updraft base.

Our model is illustrated schematically in Fig. 2. Warm pool quantities are denoted by the subscript  $w$ , cold pool quantities by  $c$ , and quantities within the updraft region by  $u$ . Within the updraft, a large fraction of the condensed moisture falls to the surface as precipitation. The remainder detrain at the tropopause, reevaporating and moistening the air that descends toward the boundary layer. The updraft is a crude representation of a mesoscale convective system, which accounts for most tropical rainfall (Houze and Betts 1981). In fact, mesoscale convective systems consist of more than deep convective updrafts, including, for example, downdrafts weighted by reevaporating precipitation and extensive

high-level stratiform clouds, which produce roughly one-third of the total rainfall while significantly modifying the clear-sky radiative fluxes. For simplicity, we neglect the downdrafts in our mass budget and assume that all precipitation reaching the surface occurs beneath the updraft. However, we will attempt to include the radiative effects of the high-level clouds associated with mesoscale convective systems in our energy budget for the warm pool.

The updrafts are embedded within the warm pool, where air otherwise descends in our model. At any instant in time, convection is observed to occur over only a small fractional area of the Tropics, on the order of a few percent. Over a longer period of a month or a season, the location of this convection varies so that on a climatic timescale, a much larger fraction of the Tropics—on the order of a third to a half—undergoes frequent convection. This larger region defines the warm pool in our model, and the occurrence of convection within distinguishes it from the cold pool. The updraft region and warm pool together can be regarded as the ascending branch of the Hadley and Walker circulations, while the cold pool corresponds to the descending branch. The occurrence of convection within the warm pool will result in differing assumptions about the distribution of moisture above the boundary layer, in comparison to the cold pool distribution, as described below.

The updraft strength  $M_u$  and descent rates over the warm and cold pools,  $M_w$  and  $M_c$ , respectively, are related by the continuity equation

$$a_u M_u = a_w M_w + a_c M_c, \quad (1)$$

where  $a_u$ ,  $a_w$ , and  $a_c$  are the fractional areas of the updraft region, warm pool, and cold pool, whose sum is equal

to unity. These areas are specified for the calculations in this article, although in the final section, we will suggest how they might evolve in response to the circulation. An upward mass flux within the updraft region is defined as positive  $M_u$ , while a downward mass flux over the warm and cold pools corresponds to positive  $M_w$  and  $M_c$ . The vertical mass flux within each region is assumed to be constant between the tropopause and  $z_B$ , the lifting condensation level, while decreasing to zero at the surface. Horizontal flow into the updraft thus occurs within the layer bounded by the surface and the lifting condensation level (referred to as the ‘‘mixed’’ layer, as discussed below). While convective inflow is observed to take place over a deeper layer in the Tropics (Reed and Recker 1971; Thompson et al. 1979), confining the inflow within a shallow layer assumed to be well mixed by dry convection allows the assumption of a single convective cloud-top height, which simplifies the vertical structure of our model.

Associated with the vertical mass flux is horizontal mass exchange between the three regions, idealized in our model to occur at the tropopause, and by continuity as an equal and opposite flux within the mixed layer beneath  $z_B$ . At the tropopause, there is a horizontal flux  $a_u M_u$  from the updraft to the warm pool<sup>1</sup> with compensating flow back into the updraft region within the mixed layer below. Consistent with (1), this return flow can be decomposed into two parts: a flux  $a_w M_w$  that enters the warm pool mixed layer from above and a horizontal flux  $a_c M_c$  that enters from the cold pool mixed layer. Flow out of the cold pool is balanced by a horizontal flux  $a_c M_c$  from the warm pool at the tropopause. Since the cold pool in our model represents the descending branch of the Hadley and Walker circulations,  $a_c M_c$ , the mass flux between the warm and cold pools, measures the strength of this circulation.

Within each region, we divide the atmospheric column into two layers and, for each layer, construct budgets of dry static energy  $s = C_p T + gz$  and specific humidity  $q$ . In the upper layer, we also consider the mixing ratio  $l$  of liquid water and ice (referred to collectively as hydrometeors). Our model lacks a momentum budget, but we implicitly include dynamics by equating the temperature above the cold pool boundary layer to the warm pool value at the same level. Models of the Hadley circulation show that horizontal temperature differences are small above the boundary layer (Schneider 1977; Held and Hou 1980), a consequence of thermal wind balance and angular momentum conservation by the air detraining from the updraft region at the tropopause. The large tropical value of the Rossby radius of deformation limits temperature gradients for zonally asymmetric circulations as well. The dynamical

elimination of horizontal temperature gradients above the tropical boundary layer has been cited by Wallace (1992) and Pierrehumbert (1995) to account for the stability of surface temperatures within the warmest regions of the Tropics marked by deep convection. In fact, at the poleward edge of the Tropics, nonzero temperature gradients result from mixing by midlatitude eddies (e.g., Peixoto and Oort 1992; Pierrehumbert 1995). This suggests that the subtropical low-level static stability, upon which low cloud cover depends, is affected not only by changes in tropical temperature but by extratropical variations as well. While this suggests an important feedback worthy of consideration, it is beyond the scope of our model.

In the remainder of this section, we present budgets of dry static energy and moisture. We then make use of the small observed fractional area of the updraft region in order to simplify the model. Next, we compute vertical integrals of the budgets to illustrate the physics underlying our model. We also describe the means by which the radiative and surface fluxes are calculated. Finally, we describe the algorithm used to find solutions to our model, while summarizing the externally prescribed parameters.

#### b. Dry static energy budget

For each of the updraft, warm pool, and cold pool regions we compute the dry static energy budget. The atmospheric column within each region is divided into two layers. The first is the mixed layer, bounded by the ocean surface and the local lifting condensation level  $z_B$ , and the second extends from  $z_B$  to the tropopause. Within the mixed layer, dry static energy and moisture are assumed to be vertically uniform as a result of mixing by dry convection. Over the trade cumulus region of the subtropics (corresponding to the downwind edge of the cold pool in our model and areas of the warm pool not occupied by mesoscale cloud systems), this mixed layer is capped by a weak inversion (Augstein et al. 1974), whose height is determined by dry convective dynamics rather than the lifting condensation level. However, these heights are approximately equal, and this model will not distinguish between them.

Within the mixed layer of each region, the budgets of dry static energy are

$$a_u M_u (s_{B,u} - s_{B,w}) = a_u [R_u(z_B) - R_u(0) + S_u] \quad (2)$$

$$a_w M_w (s_{B,w} - s_{B+,w}) + a_c M_c (s_{B,w} - s_{B,c}) = a_w [R_w(z_B) - R_w(0) + S_w] \quad (3)$$

$$a_c M_c (s_{B,c} - s_{B+,c}) = a_c [R_c(z_B) - R_c(0) + S_c], \quad (4)$$

where  $S$  is the surface sensible heat flux and  $R$  is the

<sup>1</sup> Because  $a_u$  represents the *fractional* area of the updraft,  $a_u M_u$  should be multiplied by the total tropical area in order to be a true mass flux with units of  $\text{kg s}^{-1}$ .

net radiative flux (positive downward), both evaluated per unit area. The subscript  $B$  refers to the value of dry static energy within the mixed layer, while the subscript  $B^+$  denotes the dry static energy just above the mixed-layer inversion at  $z_B$ .

The dry static energy budget of the updraft mixed layer is given by (2). Air departs this layer with dry static energy  $s_{B,u}$  and is replaced by air from the warm pool that enters with dry static energy  $s_{B,w}$ . The flux divergence, equivalent to the difference of these fluxes, is denoted by the left-hand side of (2) and, along with radiative cooling of the layer, must be balanced by the surface sensible heat flux.

The flux of dry static energy out of the warm pool mixed layer is  $a_u M_u s_{B,w}$ , which, according to the continuity equation (1), can be written as  $a_w M_w s_{B,w} + a_c M_c s_{B,w}$ . This is offset by the incoming flux  $a_w M_w s_{B+,w}$ , associated with air descending through the mixed-layer inversion at  $z_B$ , and the flux  $a_c M_c s_{B,c}$  from the cold pool so that the left-hand side of (3) represents the flux divergence within the warm pool mixed layer. The left-hand side of (4) similarly gives the flux divergence within the cold pool mixed layer as the difference between the flux to the warm pool  $a_c M_c s_{B,c}$  and the incoming flux  $a_c M_c s_{B+,c}$ , associated with the subsiding air.

The difference in temperature across the mixed-layer inversion is typically less than 1 K (Augstein et al. 1974; Sarachik 1974). While this difference could be calculated (cf. Sarachik 1974), we will avoid this complication and take advantage of its small value by setting  $s_{B+,c}$  equal to  $s_{B,c}$  and  $s_{B+,w}$  equal to  $s_{B,w}$ . Consequently, the first term on the left-hand side of (3) and (4), which represents subsidence warming of the mixed layer, is set equal to zero. In contrast, subsidence warming is included in the model of Betts and Ridgway (1989). This is because the lowest layer in their model extends above the well-mixed layer to the trade inversion. Because of stable stratification above  $z_B$ , air enters their model's lowest layer at the trade inversion with a substantially higher value of dry static energy than the value with which it departs for the updraft so that subsidence warming is nonnegligible in this case.

At the top of the mixed layer, there is also a downward turbulent flux of heat, which is often parameterized in terms of the surface sensible heat flux (e.g., Tennekes 1973; Sarachik 1974). The relation between these two fluxes depends upon cloud cover (Betts and Ridgway 1989), among other variables, but because the downward flux is comparatively small, it will be neglected in this model.

Between the top of the mixed layer at  $z_B$  and the tropopause at  $z_T$ , the budgets of dry static energy are

$$\begin{aligned} & a_u M_u (s_T - s_{B,u}) \\ & = a_u [R_u(z_T) - R_u(z_B) + L(P + M_u l_{T,u})] \end{aligned} \quad (5)$$

$$\begin{aligned} & a_w M_w (s_{B,w} - s_T) \\ & = a_w [R_w(z_T) - R_w(z_B) - M_w l_{T,w} - LR_w] \end{aligned} \quad (6)$$

$$\begin{aligned} & a_c M_c (s_{B,c} - s_T) \\ & = a_c [R_c(z_T) - R_c(z_B) + F_{m,s} - M_c l_{T,c} - LR_c], \end{aligned} \quad (7)$$

where the subscript  $T$  refers to the tropopause values of dry static energy  $s_T$ , along with the hydrometeor (i.e., liquid water and ice) mixing ratio  $l_{T,u}$ . Precipitation that reaches the surface is  $P$ , and cooling by the reevaporation of hydrometeors descending from the detrainment level over the warm and cold pools is given by  $a_w M_w l_{T,w}$  and  $a_c M_c l_{T,c}$ , respectively. As described below with the moisture budget, reevaporating hydrometeors are divided into two categories: those small enough to be carried by the large-scale circulation, whose flux is denoted by  $a_w M_w l_{T,w}$  and  $a_c M_c l_{T,c}$ , and those larger hydrometeors that fall at a much faster speed and whose flux is denoted by  $a_w LR_w$  and  $a_c LR_c$ . Radiative cooling at the tropopause is assumed to be sufficiently small so that the dry static energy is unchanged as air detrains from the updraft region and moves laterally toward the warm and cold pools.

Within the updraft, latent heat release balances cooling by adiabatic expansion and radiation, as represented by (5). The condensed water consists of precipitation  $a_u P$ , which falls to the surface, and the flux of hydrometeors  $a_u M_u l_{T,u}$ , which leave the updraft at the tropopause. (The difference between the latent heats of condensation and sublimation is ignored.)

Over the warm and cold pools, subsidence warming balances cooling by radiation, reevaporation of hydrometeors detrained by the updraft, and the divergence of the eddy transport of dry static energy, denoted by  $F_{m,s}$  in (7). This transport is approximately equal to the poleward heat flux since the eddies are quasi-horizontal (cf. Fig. 13.7 from Peixoto and Oort 1992). We approximate this divergence as occurring entirely within the cold pool (cf. Fig. 13.5 of Peixoto and Oort 1992) so that  $F_{m,s}$  equals the total tropical eddy flux divergence normalized by the cold pool area. Eddy transport is observed to occur throughout the entire depth of the troposphere but, because our mixed layer is comparatively thin, we will assume for simplicity that the transport occurs entirely between  $z_B$  and the tropopause.

### c. Water vapor and hydrometeor budgets

Budgets of moisture are constructed by dividing the atmospheric column into two layers, as for the dry static energy budgets. Within the updraft region, the lower layer extends from the surface to the lifting condensation level  $z_B$ , as before. Over the warm and cold pools, however, the lower layer is defined to extend from the surface to the top of the trade inversion at  $z_T$ . Recall that for the budgets of dry static energy, the lower layer over the warm and cold pools extends only to the lifting condensation level  $z_B$ . The use of different lower-layer thicknesses for the dry static energy and moisture budgets is an accounting shortcut and does not represent any approximation. (We could have defined the top of

the lower layer as  $z_B$  for budgets of both moisture and dry static energy. If we then constructed the moisture budget for the layer extending from  $z_B$  to the trade inversion, and combined this with the mixed layer moisture budget, we would have arrived at the same equations described below.)

The moisture budgets for the lower layer are

$$a_u M_u (q_{B,u} - q_{B,w}) = a_u E_u \quad (8)$$

$$a_w M_w (q_{B,w} - q_{TI,w}) + a_c M_c (q_{B,w} - q_{B,c}) = a_w E_w \quad (9)$$

$$a_c M_c (q_{B,c} - q_{TI,c}) = a_c E_c + a_c F_{m,q}, \quad (10)$$

where the subscript TI refers to the value of specific humidity at the trade inversion. The evaporation rate  $E$  and the divergence of the eddy moisture flux  $F_{m,q}$  are evaluated per unit area. Eddy divergence of moisture is assumed to occur entirely within the cold pool, as before, and is neglected above the trade inversion.

Beneath the updraft, the divergence of the moisture flux within the lower layer, represented by the left-hand side of (8), is balanced by evaporation. Over the warm and cold pools, evaporation moistens the dry air subsiding through the trade inversion, while balancing the horizontal advection of drier air from the cold pool into the warm pool and the mixing of dry air into the cold pool by midlatitude eddies.

Moisture subsiding through the trade inversion is assumed to have entered the upper troposphere by detraining from the updraft region at the tropopause (Sun and Lindzen 1993a):

$$a_w M_w q_{TI,w} + a_c M_c q_{TI,c} = a_u M_u (q_{T,u} + l_{T,u}). \quad (11)$$

The right-hand side of (11) represents the amount of moisture that must detrain from the convective updrafts at the tropopause in order to supply the moisture that descends through the trade inversion, given by the left-hand side of the equation. Since  $q_{T,u} \ll q_{TI,w}, q_{TI,c}$ , as a result of the relatively cold temperature at the tropopause, the detraining moisture consists largely of hydrometeors  $l_{T,u}$ . Consequently, not all the moisture condensing within the updraft reaches the surface as precipitation.

We will not attempt to compute in detail the distribution of moisture above the trade inversion. Instead, we will specify vertical profiles of relative humidity for the warm and cold pools, respectively, as described below in conjunction with the radiative flux calculation. Here, we construct budgets of moisture above the trade inversion in order to identify the physical processes controlling the moisture distribution within this layer and motivate our choice of relative humidity profile. In particular, we wish to show why the cold pool upper troposphere is drier than the corresponding region over the warm pool—that is, what processes controlling moisture allow the “radiator fins” of Pierrehumbert (1995) to emerge.

Hydrometeors detraining at the tropopause have fall speeds on the order of a few tens of centimeters per second (Heymsfield and Donner 1990), which is much larger than the rate of large-scale subsidence, typically of order  $1 \text{ cm s}^{-1}$ . Given a flux of hydrometeors out of the updraft equal to  $a_u M_u l_{T,u}$ , we will assume that most precipitate out of the large-scale flow and denote this loss as  $-a_w R_w$ . However, we will assume that some hydrometeors are small enough to be carried along with the large-scale flow into the warm pool free troposphere and the cold pool, and write this flux as  $a_w M_w l_{T,w} + a_c M_c l_{T,w}$ , or equivalently  $a_u M_u l_{T,w}$ , because of (1). Thus, the budget of hydrometeors at the warm pool tropopause is

$$a_u M_u (l_{T,w} - l_{T,u}) = -a_w R_w. \quad (12)$$

We have assumed that the temperature of the tropopause is horizontally uniform so that water vapor does not condense while at this level and we also assume that reevaporation of hydrometeors begins only after they have descended beneath the tropopause. Consequently, the specific humidity of the detraining air remains unchanged at this level so that the water vapor budget at the warm pool tropopause is

$$a_u M_u (q_{T,w} - q_{T,u}) = 0 \quad (13)$$

and  $q_{T,w}$  is equal to  $q_{T,u}$ . Similarly, the hydrometeor and water vapor budgets over the cold pool tropopause are

$$a_c M_c (l_{T,c} - l_{T,w}) = -a_c R_c \quad (14)$$

$$a_c M_c (q_{T,c} - q_{T,w}) = 0, \quad (15)$$

so  $q_{T,c}$  is equal to  $q_{T,w}$  and  $q_{T,u}$ . Because the characteristic hydrometeor fall speed is so large, we expect most hydrometeors to precipitate out over the warm pool close to convective towers. (Given a typical fall speed of a few tens of centimeters per second and a horizontal detrainment velocity of  $5 \text{ m s}^{-1}$ , the hydrometeors will rejoin the surface flow within a degree or two of the updraft.) Consequently, only convective towers on the fringes of the warm pool can be expected to contribute to  $R_c$ .

All hydrometeors are assumed to reevaporate completely before they reach the trade inversion. Thus, between the tropopause and trade inversion, the budgets of water vapor for the warm and cold pools are

$$a_w M_w (q_{TI,w} - q_{T,w}) = a_w (R_w + M_w l_{T,w}) \quad (16)$$

$$a_c M_c (q_{TI,c} - q_{T,c}) = a_c (R_c + M_c l_{T,c}). \quad (17)$$

Horizontal mixing by tropical and midlatitude synoptic-scale eddies tends to dry out the Tropics (Yang and Pierrehumbert 1994). However, based on the observed zonally averaged transient-eddy moisture flux from Fig. 12.11 of Peixoto and Oort (1992), the divergence is estimated to be small compared to the detraining flux of hydrometeors, and we will neglect the eddy flux divergence above the trade inversion.

As a result of (14) through (17), it can be shown that

TABLE 1. Annual-average deep convective cloud cover according to ISCCP and the fraction of the Tropics with greater than average convective cloud cover (denoted by  $a_w$ , in percent) for each season.

Season	Average	$a_w$
DJF	4.80	39
MAM	4.32	39
JJA	4.50	37
SON	4.81	41

$$q_{TL,w} - q_{TL,c} = \frac{R_w}{M_w} > 0. \quad (18)$$

Detained hydrometeors that precipitate out over the warm pool are unavailable to moisten the cold pool, resulting in a warm pool upper troposphere that is relatively moist. This is the origin of the radiator fins in our model—that is, the cold pool region that is relatively transparent to infrared radiation as a result of its dearth of water vapor (Pierrehumbert 1995). The cold pool is relatively dry because the air subsiding within has been depleted of moisture by the precipitation of hydrometeors during its journey over the warm pool. In contrast, the warm pool is relatively opaque to infrared radiation due to its proximity to the updraft region that is the source of upper-tropospheric moisture in our model.

Finally, we can write the moisture budget for the updraft between cloud base and the tropopause as

$$a_u M_u (q_{T,u} + l_{T,u} - q_{B,u}) = -a_u P. \quad (19)$$

The change in total water between cloud base and cloud top equals the precipitation that falls to the surface beneath the updraft.

#### d. The 2½-box limit

As noted by Riehl and Malkus (1958), deep convection is observed to occur as isolated “hot towers,” and the ISCCP tropically averaged deep convective cloud cover (shown for each season in Table 1) is between 4% and 5% so that  $a_u \ll a_w, a_c$ . Thus, to a good approximation, we can simplify our model by taking the limit of  $a_u \rightarrow 0$ , with  $a_u M_u$  and  $a_u P$  remaining nonzero. That is, the total upward mass flux and precipitation rate are assumed to remain nonzero as the updraft region becomes infinitely narrow.

In this limit, Eqs. (2), (8), (5), and (19) become

$$s_{B,u} = s_{B,w} \quad (20)$$

$$q_{B,u} = q_{B,w} \quad (21)$$

$$a_u M_u (s_T - s_{B,u}) = a_u L(P + M_u l_{T,u}) \quad (22)$$

$$a_u M_u (q_{T,u} + l_{T,u} - q_{B,u}) = -a_u P \quad (23)$$

so that

$$\boxed{s_T + Lq_{T,u} = s_{B,w} + Lq_{B,w}} \quad (24)$$

Thus, in the limit  $a_u \rightarrow 0$ , the warm pool boundary layer

and tropopause are connected by a moist adiabat. The physical interpretation suggested by our model is as follows. As the updrafts become infinitely narrow, advective fluxes into and out of the updraft column dominate the radiative and surface fluxes. Equilibrium requires that the net advective flux be zero, that is, that the import and export values of moist static energy  $h$  (defined as  $s + Lq$ ) be identical. The result (24) was found in the single-box model of Sarachik (1978), and our model suggests that it should be interpreted as a consequence of the implicit negligible extent of the updraft in that model.

If we assume that air at the top of the updraft is saturated, so that  $q_{T,u}$  is determined by  $s_T$ , then the tropopause dry static energy can be derived using (24) in terms of the thermodynamic properties of the mixed layer overlying the warm pool. This same constraint can also be applied to the model of Pierrehumbert (1995); thus, the difference  $s_T - s_{B,c}$  (there denoted by  $\delta\theta$ ) can be derived as part of the model solution, rather than specified as an external parameter.

#### e. Energy integrals

We add a surface energy budget,

$$R_w(0) - LE_w - S_w + F_{o,w} = 0 \quad (25)$$

$$R_c(0) - LE_c - S_c + F_{o,c} = 0, \quad (26)$$

where  $F_{o,w}$  and  $F_{o,c}$  represent the divergence of energy per unit area within the warm and cold pools by the ocean circulation. Then it can be shown by summing over the vertical layers of the warm pool that

$$\begin{aligned} a_w R_w(z_T) &= -a_w F_{o,w} \\ &+ a_c M_c (s_T + Lq_{T,u} - s_{B,c} - Lq_{B,c}) \\ &= -a_w F_{o,w} + a_c M_c (h_T - h_{B,c}), \end{aligned} \quad (27)$$

where  $h_T$  is the moist static energy at the tropopause, equal to  $s_T + Lq_{T,u}$ . The net gain of radiative energy by the warm pool must be balanced by atmospheric export of moist static energy or else ocean heat transports, as noted by Pierrehumbert (1995). The quantity  $h_T - h_{B,c}$  is identical to the “gross moist stability” derived by Neelin and Held (1987), who noted that in order for a direct circulation to export energy from an atmospheric column, the moist static energy must be larger in the outflow branch of the circulation.

The large-scale circulation in our model,  $M_c$ , is driven by the total energy gain of the warm pool. According to (27), this gain is a balance between radiation and the divergence of ocean transports but does not include latent heating. Consider for simplicity the tropical atmosphere in the absence of ocean transports and imagine a case where the warm pool upper troposphere is dry enough so that all incoming radiation can be reradiated locally: that is, consider  $R_w(z_T)$  equal to zero. Equation (27) can be satisfied by setting  $M_c$  identically equal to

zero. Latent heat will still occur within the warm pool in order to balance the divergence of the radiative flux between the tropopause and the surface, but convective ascent will be balanced locally by  $M_w$ . The point is that despite considerable latent heat release,  $R_w(z_T)$  and  $M_c$  are zero so that there is no large-scale circulation extending throughout the Tropics. This example suggests that it is not latent heating that drives the large-scale circulation, but instead the radiative gain in the deep Tropics (Emanuel et al. 1994). Of course, this radiative gain is partly due to the moisture content high above the warm pool, which increases the longwave opacity and is supplied by convection. Thus, convection may drive the large-scale circulation, but only by moistening the warm pool upper troposphere and creating a net radiative gain, rather than through latent heat release.

Convection influences the large-scale circulation by determining the lapse rate (Emanuel et al. 1994). The existence of isolated convective towers requires that the moist static energy at the tropopause and warm pool surface be identical so that, together, (24) and (27) imply that

$$a_w R_w(z_T) = -a_w F_{o,w} + a_c M_c (h_{B,w} - h_{B,c}). \quad (28)$$

The moist static energy export from the warm pool is proportional to the difference in the surface values of moist static energy between the warm and cold pools. If the surface relative humidity in the Tropics is roughly uniform, then  $q$  should be an increasing function of the surface temperature  $T_s$  so that  $h$  is also an increasing function of  $T_s$ . Thus, according to (28), energy export from the warm pool requires that

$$\boxed{T_{s,w} > T_{s,c}}. \quad (29)$$

Thus, the assumption of descent over the cold pool ( $M_c > 0$ ), requires that this region be relatively cool: the circulation is necessarily direct. This is essentially an expression of the Second Law of Thermodynamics by the model.

#### f. Boundary layer and radiation models

The surface sensible heat flux and evaporation rate remain to be specified. Following Pierrehumbert (1995), we constrain the surface fluxes by setting  $T_s = \text{SST} - 1.0$  K and requiring that the surface relative humidity equal 75% (or some other reasonable value). While this removes from our model the ‘‘ventilation’’ feedback proposed by Hartmann and Michelsen (1993), whereby warming of the convective region is offset by increased evaporation resulting from an invigorated large-scale circulation, it nonetheless results in realistic boundary layer values of temperature and humidity that are important to the radiative calculation. [We have subsequently parameterized the surface fluxes using bulk formulas as in Betts and Ridgway (1989) and found the

same low cloud cover feedback as described in section 4.]

The difference between atmospheric surface temperature and the underlying SST is observed to increase away from the convecting region (e.g., Pierrehumbert 1995), and as a sensitivity calculation, we computed solutions with this difference increased by an extra degree over the cold pool. Atmospheric temperature was virtually unchanged as a result, with the surface value over both the warm and cold pools decreasing by less than 0.1 K. Instead, the prescribed increase in the cold pool air–sea temperature difference was compensated by an increase in cold pool SST of slightly less than a degree. The value of SST in the model appears to be unimportant to the equilibrium climate and is determined by the temperature of the overlying atmosphere. Pierrehumbert (1995) argues that at tropical temperatures, the warm pool atmosphere is so humid and opaque to longwave radiation that the longwave flux at the TOA [outgoing longwave radiation (OLR)] is nearly independent of the SST below. Consequently, it is changes in the atmospheric temperature, rather than SST, that allow the OLR to adjust to changes in forcing. This appears to also be true for the cold pool boundary layer in our model.

The radiative fluxes are calculated using the Goddard Institute for Space Studies (GISS) radiation model (Hansen et al., 1983). Model resolution is 100 m within the first 2 km and above this height increases exponentially up to the highest model level at 100 km, with a total of 39 levels. The radiation model requires as input the vertical profiles of temperature and moisture along with cloud cover and cloud optical thickness. How clouds affect the radiative fluxes is described in sections 3 and 4. The warm pool temperature is assumed to be characterized by a moist adiabat arising from the mixed layer, consistent with (24). While the observed temperature profile more closely fits a moist adiabat when virtual effects are included (Betts 1982; Xu and Emanuel 1989), this distinction will be neglected. We also assume that the cold pool temperature above the trade inversion is given by this same adiabat since horizontal temperature gradients within the Hadley circulation are small (Schneider 1977; Held and Hou 1980).

The top of the trade inversion over the warm pool,  $z_{\text{TI},w}$ , is prescribed at 2 km (Riehl 1979). Over the descending branch of the Hadley circulation, the inversion top is observed to vary from less than 1 km at the upwind edge of the subtropical cloud decks to near 2 km as the trade winds approach the convecting region, and we take  $z_{\text{TI},c}$  equal to 1.5 km as a representative value. We find that increasing  $z_{\text{TI},c}$  to 2 km causes both the warm and cold pools to rise in temperature by roughly a degree since the deeper boundary layer corresponds to a larger column-integrated water content, increasing the opacity above the cold pool surface.

Between the mixed layer (bounded in the model by the lifting condensation level) and the trade inversion,

thermodynamic properties reflect a mixture of surface air along with air subsiding through the inversion (e.g., Betts and Albrecht 1987; Boers and Betts 1988). Following Betts and Ridgway (1989), the temperature and moisture structure within this layer are assumed to lie along a mixing line. This requires that mixing between air descending through the inversion and mixed-layer air is conservative, which given the observed presence of radiative cooling, precipitation, and reevaporation is not strictly true. Nonetheless, it gives a vertical structure close to that observed and has the advantage that the profile depends upon properties of both the boundary layer and subsiding air. We compute the mixing fraction of surface and subsiding air by setting the mixing parameter  $\beta \equiv dp^*/dp$  equal to 1.2. This parameter measures how rapidly the saturation pressure  $p^*$  of the mixture varies with actual pressure  $p$  (Betts 1982). For  $\beta$  equal to unity, the mixture is just saturated at all levels. The value of  $\beta$  equal to 1.2 is based upon observations of subtropical clear-sky regions by Betts and Albrecht (1987). Since  $\beta$  is specified to be greater than unity, the saturation pressure increases with height faster than the actual pressure of the mixture, and the mixture is increasingly far from saturation as the trade inversion is approached from below. The mixing line model is used to compute temperature and humidity up to the inversion base. The inversion thickness is specified as 200 m and, within the inversion, temperature and moisture are specified using linear interpolation between the mixing line below and the warm pool moist adiabat above.

In theory, the moisture structure above the trade inversion depends upon such cloud microphysical parameters as the precipitation efficiency of the deep convective clouds along with the precipitation and reevaporation rates of the detraining air (Sun and Lindzen 1993a). In addition, lateral mixing by both tropical and extratropical transients influences the horizontal distribution of moisture (Yang and Pierrehumbert 1994). Inclusion of these processes would result in a more complicated model than is practical. For simplicity, we assume that relative humidity above the trade inversion decreases linearly with pressure, following Manabe and Weatherald (1967). Above the warm pool inversion, relative humidity falls off linearly with respect to the surface value. Over the cold pool inversion, relative humidity decreases with respect to the trade inversion value that is specified as an external parameter of the model. As a consequence, upper-tropospheric moisture over the warm pool increases with the warm pool surface temperature, while upper-tropospheric moisture over the cold pool is held fixed.

This distinction is motivated by the analysis of observed tropical relative humidity by Sun and Oort (1995), wherein interannual variations in warm pool surface temperature are found to be correlated with increased upper-tropospheric moisture directly above, but uncorrelated with upper-tropospheric moisture over the subtropics (represented by the cold pool in our model).

One interpretation is that increased convection in response to rising surface temperature moistens the overlying troposphere by increasing the supply of detrained hydrometeors. It is perhaps more appropriate to parameterize upper-tropospheric moisture in terms of the model's detrained hydrometeor content  $l_{T,u}$  or precipitation  $P$  instead of surface temperature, but all these fields have roughly the same dependence upon our model external parameters (cf. Fig. 6), and we will overlook this distinction. Sun and Oort show that the increase in tropically averaged moisture at any level in response to warming is overestimated by a constant relative humidity model. If this result holds for the warm pool alone, then the clear-sky greenhouse feedback is overestimated by the model in this region. Nonetheless, use of a constant relative humidity profile simplifies calculation of the vertical moisture profile, and it is assumed to be sufficiently realistic, given our limited goal of estimating the feedback due to low cloud cover.

In the moisture budget presented previously, the relative humidity at the tropopause is necessarily 100% since the air arriving at this level is saturated upon detraining from the convective updraft and contains hydrometeors. This contradicts the decrease of relative humidity with height assumed by the radiative model. We resolve this inconsistency by assuming that there is some intrusion of dry midlatitude air by eddies that reduces the tropopause humidity to subsaturated values assumed by the radiative calculation (Yang and Pierrehumbert 1994). To be rigorous, we should add a moisture sink at the tropopause so that this process can be balanced by increased surface evaporation. However, the saturation vapor pressure is so small at the tropopause that only a small moisture sink is required to reduce the humidity below saturation, and omission of this process results in only a small error in the surface evaporation.

Above the tropopause, the stratospheric temperature is specified at 195 K. This temperature could be calculated as a function of the solar constant, given the concentration of solar absorbers (e.g., Lindzen et al. 1982), but we will simply impose its value and assume that it depends negligibly upon the tropospheric circulation below (cf. Sarachik 1978; Betts and Ridgway 1989). Solar fluxes are calculated assuming the warm and cold pools to be  $4^\circ$  and  $20^\circ$  of latitude off the equator, respectively. For each radiative profile, we sample the annual cycle one day per month, using three solar angles on each day between sunrise and noon in order to sample the diurnal cycle. This allows us to take into account the nonlinear dependence of ocean albedo upon solar zenith angle, although given the idealizations made in the remainder of our tropical model, we probably could have done just as well (and saved some CPU) by computing the solar fluxes using an annual-mean solar zenith angle.

### g. Midlatitude exports

Export of dry static energy and moisture to mid-latitudes by atmospheric eddies and ocean transports is prescribed in the model based upon present-day observed values (Peixoto and Oort 1992). The divergence of ocean transport across 30°N and 30°S is estimated from their Fig. 13.17 as  $6 \times 10^{15}$  W. This cooling is assumed to be evenly distributed over the Tropics, equivalent to  $-23.6$  W m<sup>-2</sup>.

Atmospheric eddy transports account for approximately an additional  $5 \times 10^{15}$  W of cooling. This export is partitioned into tropically averaged cooling rates of  $-8.6$  W m<sup>-2</sup> by dry static energy transports and  $-10.2$  W m<sup>-2</sup> ascribed to latent heat export. Figure 13.11 of Peixoto and Oort (1992) shows that transient and eddy transports are nearly zero within roughly 15° latitude of the equator. As noted above, we approximate atmospheric exports to occur entirely within the model cold pool so that  $F_{m,s}$  and  $LF_{m,q}$  are set equal to the above values divided by the cold pool fractional area.

### h. Algorithm

To find solutions to the model, we begin by guessing values for  $T_{s,w}$  and  $T_{s,c}$ , the surface temperatures of the warm and cold pools. The mixed-layer specific humidities  $q_{B,w}$  and  $q_{B,c}$  can be computed using the prescribed values of surface relative humidity. Using  $T_{s,w}$  and  $q_{B,w}$ , we construct the moist adiabat linking the warm pool mixed layer and the tropopause. The height of the tropopause,  $z_T$ , occurs at that level where the moist adiabatic temperature equals the prescribed stratospheric temperature. We also solve for  $q_{T,u}$ , assuming that air is saturated at the cloud top. Given our assumption of horizontally uniform temperatures, the adiabat gives temperature everywhere above the trade inversion. Using the mixing line model, we can compute the temperature and moisture profiles between  $z_B$ , the top of the mixed layer (computed as the lifting condensation level), and the prescribed trade inversion height  $z_{TI}$ .

Given our guessed surface temperatures, we have derived temperature at every level along with the specific humidity, given  $q_{TI,c}$  and the assumption that relative humidity decreases linearly with pressure above the trade inversion. (An example of the vertical structure of temperature and specific humidity is shown in Fig. 3.) This allows us to calculate the clear-sky radiative fluxes, along with the cloud forcing, which is either prescribed as in section 3, or calculated as in section 4 and appendix A.

Using (6), (13), and (16), along with (7), (15), and (17), we can solve for the subsidence rates  $M_w$  and  $M_c$ . Next, we solve for the surface sensible heat fluxes,  $S_w$  and  $S_c$ , using the mixed-layer dry static energy balances (3) and (4). Similarly, we solve for the surface evaporation,  $E_w$  and  $E_c$ , using the lower-layer moisture balances (9) and (10). Finally, we check whether the de-

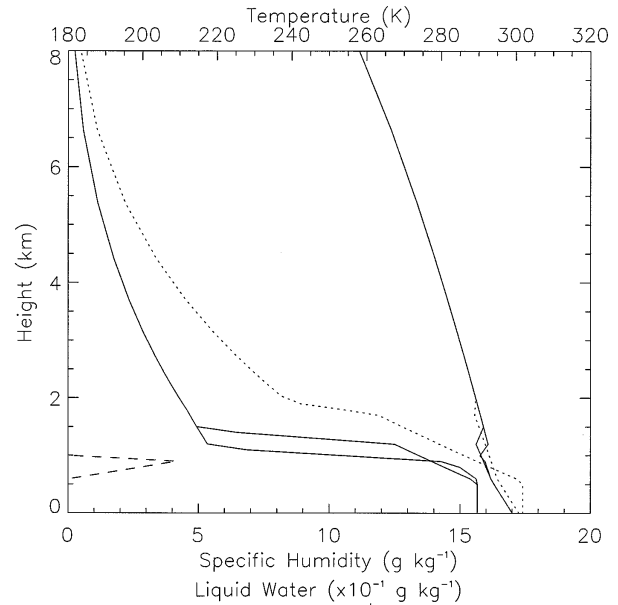


FIG. 3. Sample vertical profiles of temperature and specific humidity for the warm (dotted) and cold (solid) pools. There are two sets of profiles shown for the cold pool; the set exhibiting the lower inversion corresponds to the cloudy profile and is used only in the calculation of cloud radiative forcing described in appendix A. Cloud liquid water (dashed) is multiplied by 10.

riated surface latent and sensible heat fluxes, along with the surface radiative fluxes and the prescribed ocean heat transports, satisfy the surface energy budgets (25) and (26). If not, our initial guesses for  $T_{s,w}$  and  $T_{s,c}$  were incorrect, and we have to choose new values and iterate until (25) and (26) are satisfied. In summary, solving our simple tropical model is a root finding problem consisting of two transcendental equations, (25) and (26), with two unknowns,  $T_{s,w}$  and  $T_{s,c}$ .

The independent variables of our model are  $a_w$ , the relative size of the warm pool, and  $q_{TI,c}$ , the specific humidity at the trade inversion of the cold pool. In addition, we have to specify, as external parameters  $F_{m,s}$  and  $F_{m,q}$ , the midlatitude eddy exports of dry static energy and moisture from the cold pool that appear in (7) and (10), respectively, along with the ocean heat transports,  $F_{o,w}$  and  $F_{o,c}$ , in (25) and (26), respectively. Finally, for each region, we must specify the surface relative humidity, the air-sea temperature difference  $T_s - SST$ , and  $z_{TI}$ , the top of the trade inversion. The external variables are summarized in Table 2.

### 3. Low clouds in the present-day tropical climate

In this section, Earth Radiation Budget Experiment (ERBE) estimates of cloud radiative forcing are applied to the model in an effort to reproduce the current tropical climate. In the first experiment, cloud forcing is absent but energy export to midlatitudes by atmospheric eddies and ocean transport is specified at presently observed

TABLE 2. Summary of prescribed parameters and independent variables. Any departures from the values listed above are noted in the text.

	Symbol	Value
Prescribed variables		
Divergence by ocean heat transport		
warm pool	$F_{o,w}$	$-23.6 \text{ W m}^{-2}$
cold pool	$F_{o,c}$	$-23.6 \text{ W m}^{-2}$
Divergence of atmospheric eddy dry static energy transport		
warm pool	—	—
cold pool	$F_{m,s}$	$(-8.6/a_c) \text{ W m}^{-2}$
Divergence of atmospheric eddy latent heat transport		
warm pool	—	—
cold pool	$LF_{m,q}$	$(-10.2/a_c) \text{ W m}^{-2}$
Surface relative humidity		
warm pool	$r_w$	75%
cold pool	$r_c$	75%
Air-sea temperature difference		
warm pool	$T_{s,w} - \text{SST}_w$	$-1.0\text{K}$
cold pool	$T_{s,c} - \text{SST}_c$	$-1.0\text{K}$
Trade inversion height		
warm pool	$z_{\text{TI},w}$	2.0 km
cold pool	$z_{\text{TI},c}$	1.5 km
cold pool cloud (see appendix A)	$z_{\text{TI},cl}$	1.2 km
Independent variables		
Cold pool specific humidity at the trade inversion	$q_{\text{TI},c}$	
Warm pool fractional area	$a_w$	

values. Figure 5a shows SST for the warm and cold pools as a function of  $q_{\text{TI},c}$ , the specific humidity at the cold pool trade inversion. This value is a measure of upper-tropospheric moisture over the cold pool, since it is used to prescribe model relative humidity above the inversion. A “typical” observed value of  $q_{\text{TI},c}$  is between 4 and 5 g kg<sup>-1</sup> (Augstein et al. 1974; Klein et al. 1995; Albrecht et al. 1995). Model SST is also shown as a function of the warm pool fractional area  $a_w$ . One way to estimate the observed value of this parameter is to compute a tropical average of ISCCP deep convective cloud cover and assign  $a_w$  to the percentage of the Tropics having convective cloud cover above this value. Ta-

ble 1 shows the tropical average cloud cover and corresponding estimate of  $a_w$  for each of the seasons. Although the location of convection changes throughout the year, the areal extent of this region is nearly invariant, corresponding to  $a_w$  around 0.4. Figure 4 shows the average deep convective cloud cover for the Northern Hemisphere summer. Over most of the Tropics, the contours denoting the seasonally averaged cloud fraction and one-half this value are nearly coincident, indicating that the distinction between the convecting and nonconvecting regions is fairly precise. Other methods of estimating the extent of the warm pool can be imagined—applying the above calculation to tropical rainfall

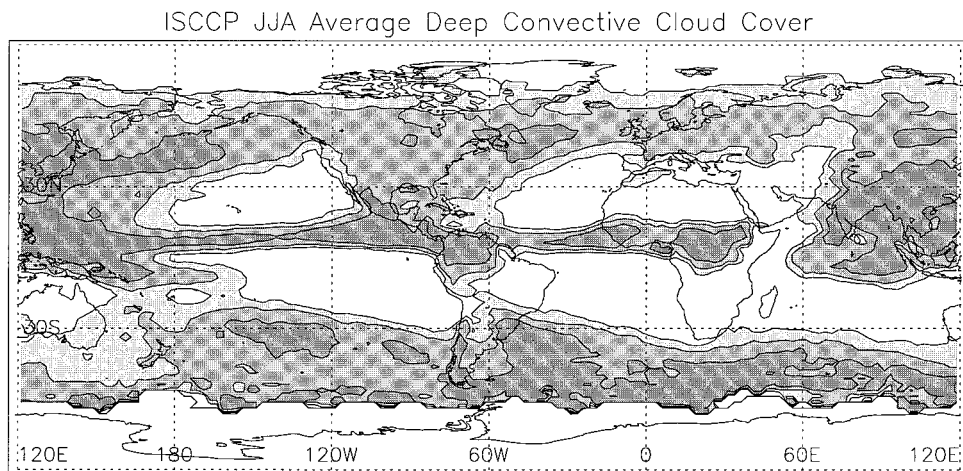


FIG. 4. Seasonal average (JJA) of ISCCP deep convective cloud cover. The tropical mean is 4.50%, and the contours are at 0.5, 1.0, and 2.0 times the mean.

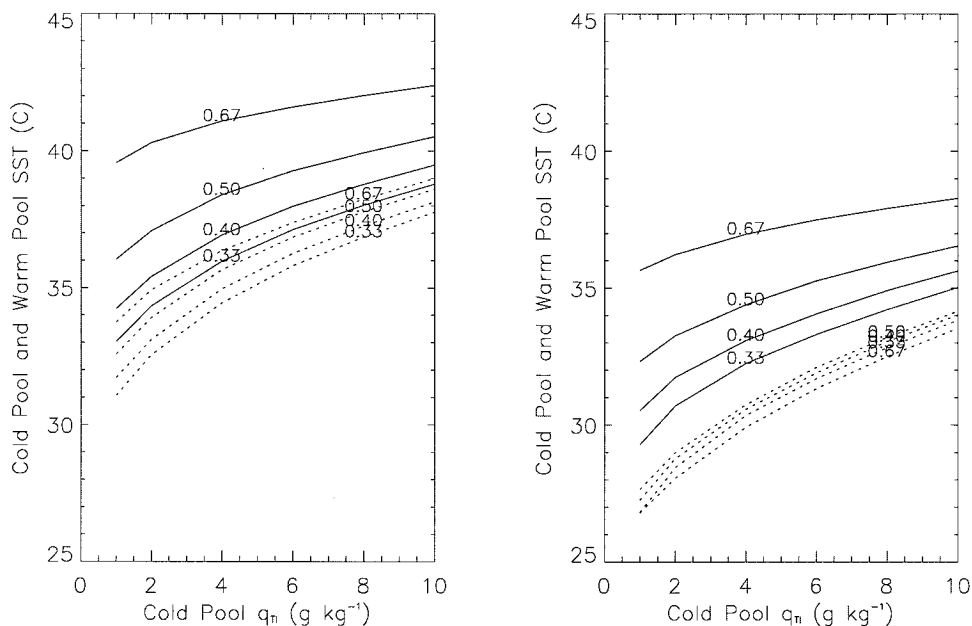


FIG. 5. Warm pool (solid) and cold pool (dotted) SST, given observed energy export to midlatitudes by atmospheric eddies and ocean transports. (a) No cloud forcing and (b) low cloud forcing of  $-15/a_c$   $\text{W m}^{-2}$  over the cold pool. Each curve represents a different value of the fractional area corresponding to the warm pool.

or upper-tropospheric moisture, for example—and we might expect that  $a_w$  be reasonably specified as small as one-third and as large as one-half.

For  $q_{\text{TL},c}$  equal to  $5 \text{ g kg}^{-1}$  and  $a_w$  given the value of 0.4, the warm pool SST is near  $37^\circ\text{C}$ . In order to reproduce present-day temperatures, cloud radiative forcing must be taken into account by the model. This may be done implicitly, through a reduction in the solar constant (e.g., Sarachik 1978), or explicitly, by computing or else prescribing cloud properties along with the corresponding radiative perturbation. For example, Betts and Ridgway (1989) prescribe 25% low cloud cover, roughly consistent with ISCCP observed values, and compute the optical thickness of these clouds using a mixing line model for the cloud temperature, specific humidity, and liquid water content, with the mixing line parameters taken from observations of trade cumuli.

In this section, the effect of clouds is estimated using ERBE observations of cloud radiative forcing at the top of the atmosphere. Cloud radiative forcing is defined as the perturbation to clear-sky fluxes resulting from the presence of clouds. For low clouds, this is estimated to be between  $-10$  and  $-15 \text{ W m}^{-2}$  during the two solstitial seasons (Hartmann et al. 1992). What remains is to relate this TOA value to cloud forcing at levels in the model where the radiative flux is needed: in particular, at the surface, the top of the subcloud layer, and the tropopause. For now, low cloud forcing will be approximated as independent of height. This is equivalent to assuming that the divergence of the radiative flux is unaffected by low clouds. Clouds modify this diver-

gence by absorbing and reemitting longwave radiation from the surface, although for low clouds this effect is small since the radiation is reemitted at temperatures that are close to those at the surface. Cloud absorption of solar radiation also contributes to radiative flux divergence. Norris and Leovy (1994) show that the effects of solar and longwave absorption upon the surface flux are somewhat offsetting, so that the value of cloud forcing at the surface is nearly that measured at the top of the atmosphere by ERBE. In appendix A, cloud forcing at each height is calculated more accurately using the GISS radiation model along with a simple model of cloud properties, and essentially the same results are found, demonstrating the validity of the approximations. These approximations were made implicitly by Philander et al. (1996), who reduced the solar flux at the ocean surface over regions of stratus cloud cover in a coupled GCM.

Figure 5b shows SST for the warm and cold pools, assuming that low-cloud forcing of  $-15/a_c \text{ W m}^{-2}$  occurs entirely over the cold pool (thus corresponding to a tropically averaged value of  $-15 \text{ W m}^{-2}$ , consistent with ERBE). Although low clouds reduce the incoming radiation only locally, within the cold pool, the temperature is reduced by a nearly equal amount over the warm pool. This demonstrates how a radiative perturbation in one part of the Tropics can alter surface temperatures in remote regions as a result of coupling by the large-scale circulation (in our model, represented by  $M_c$ ). As clouds reduce the cold pool surface temperature, the difference between the warm and cold pool moist

static energy is increased. This increases the moist static energy export from the warm pool so that this region cools along with the subtropical region directly beneath the low clouds.

Despite the lowering of tropical temperatures by low clouds, warm pool temperatures remain a few degrees above observed values. We have found that an additional tropically averaged forcing of  $-10$  to  $-15 \text{ W m}^{-2}$  is needed to bring the warm pool temperature to the current-day value near  $30^\circ\text{C}$ , given our choices of  $q_{\text{TL},c}$  and  $a_w$ . This leads us to consider what processes are missing that could reduce the model temperatures to present-day values. Cloud forcing by mid- and high-level clouds associated with deep convection has so far been neglected. These clouds can be optically thick and highly reflective, although the TOA shortwave forcing is largely offset by the longwave component (e.g., Kiehl 1994). Based upon the analyses of Hartmann et al. (1992) for the solstitial seasons, we estimate that the tropically averaged TOA cooling corresponding to midlevel clouds is on the order of a few watts per square meter, while the forcing associated with high-level cirrus and cirrostratus is as large as  $-5 \text{ W m}^{-2}$ .

It is tempting to invoke additional cloud forcing by arguing that low-cloud forcing in the subtropics is underestimated by ERBE. One potential source of underestimation is the contamination of the clear-sky radiative fluxes by the inclusion of cloudy scenes. (ERBE cloud forcing is derived by subtracting the clear-sky flux from the total flux.) This bias of the globally averaged net cloud forcing is estimated to be a few watts per square meter (e.g., Arking 1991), although it could be argued that the error is larger in the subtropics where there are extensive regions of trade cumulus clouds. These clouds have horizontal scales on the order of a few kilometers, which is smaller than the 35-km “footprint” of the ERBE scene-identification algorithm. Consequently, the presence of trade cumuli might be difficult to detect, resulting in clear-sky estimates that are biased toward the total flux and an underestimate of the low-cloud forcing in this region (A. D. Del Genio 1996, personal communication).

Along with the  $-15/a_c \text{ W m}^{-2}$  of low-cloud forcing confined to the cold pool,  $-7/a_w \text{ W m}^{-2}$  of forcing associated with mid- and high-level convective clouds will be added to the warm pool. We will also impose an additional forcing of  $-5 \text{ W m}^{-2}$  upon both regions. Although this total is about  $10 \text{ W m}^{-2}$  larger than the total ERBE tropical cloud forcing (Hartmann et al. 1992), it is consistent with the annually averaged tropical cloud forcing of  $25\text{--}30 \text{ W m}^{-2}$  estimated by ISCCP (Rossow and Zhang 1995). While we might try to justify the additional  $-5 \text{ W m}^{-2}$  forcing in terms of uncertainties or underestimates of observed low-cloud forcing by ERBE, the fact is that this amount was chosen simply to reduce the warm pool temperature to “realistic” values near  $30^\circ\text{C}$ . In the next section, we will calculate whether feedbacks associated with low cloud cover am-

plify or diminish the model sensitivity to increasing  $\text{CO}_2$ . While unphysical corrections can distort the model sensitivity, we find that our results are not highly sensitive to this correction.

We have attempted to reduce the model temperature to reasonable values without this extra  $5 \text{ W m}^{-2}$  by adjusting various model parameters. Peixoto and Oort (1992) show that most of the observed ocean heat divergence occurs in warm pool latitudes, although there are large uncertainties in this estimate. As a sensitivity calculation, we concentrate the cooling by ocean transports entirely within the warm pool. SST in this region is reduced only by roughly  $0.5 \text{ K}$ , and cold pool temperatures become unrealistically warm.

One other process absent from the model may reduce the temperature of the warm pool without the additional  $-5 \text{ W m}^{-2}$  of cloud forcing—namely, convective downdrafts (e.g., Emanuel et al. 1994; Raymond 1994). In the latter study, a convecting circulation was established by imposing an SST difference across the model domain. As a result of downdrafts weighted and cooled by reevaporated precipitation, surface temperature at the base of the convecting region was reduced by  $2^\circ\text{C}$ . As noted in the previous section, this mechanism is absent in our model, both because downdrafts are omitted and because the air–sea temperature difference is fixed. Downdrafts associated with more elaborate convective parameterizations (e.g., Del Genio and Yao 1993) have been found to cause surface cooling within GCMs when SST is prescribed as a lower boundary condition. The question is whether downdrafts would lead to surface cooling in a model such as ours where SST is calculated rather than prescribed. Pierrehumbert (1995) argues that the tropical atmosphere is sufficiently moist and opaque to longwave radiation that the rate of OLR cooling depends upon the atmospheric temperature and is relatively insensitive to the underlying SST. It is not clear whether the inclusion of downdrafts would result in cooler temperatures over the model warm pool, since this would reduce the rate of OLR emission along with the export of moist static energy, which, according to (28), is proportional to the difference in surface temperature between the warm and cold pools. As a sensitivity experiment, we reduced the warm pool surface temperature by an additional degree compared to the underlying SST. The result was a warming of SST by nearly the same amount so that the atmosphere surface temperature, and thus the effective temperature of OLR emission (related to the surface value by a moist adiabat), was unchanged. We suspect that in the absence of prescribed SST, downdrafts cannot cool the surface unless they act to dry out the middle troposphere, thus lowering the effective level of OLR emission while maintaining the original emitting temperature (i.e., the emitting temperature in the absence of downdrafts), despite the cooling at the surface.

In addition to reducing the net radiation at the top of the atmosphere, deep convective clouds reduce the cool-

ing associated with clear-sky radiative divergence. When the TOA net radiation over convective anomalies was reduced by  $10 \text{ W m}^{-2}$  during one ENSO event, the net surface radiation was reduced by  $40 \text{ W m}^{-2}$  (Chou 1994b). This implies that the tropospheric radiative divergence was decreased by  $30 \text{ W m}^{-2}$  in response to convection. Associated with the  $7/a_w \text{ W m}^{-2}$  reduction in TOA net radiation over the model warm pool that is ascribed to convective clouds, we reduce the radiative divergence between the tropopause and the top of the subcloud layer proportionally by  $20/a_w \text{ W m}^{-2}$ . In principle, this can alter the model surface temperature since thermodynamic properties of boundary layer air reflect properties of the subsiding air in proportion to the rate of descent (cf. Betts and Ridgway 1989). Because of our simple boundary layer model, however, surface temperature and moisture are determined solely by the underlying SST and are insensitive to changes in the rate of descent.

Figure 6 shows the model solution given the combination of low and convective cloud forcing described above. For  $q_{\text{TL},c}$  equal to  $5 \text{ g kg}^{-1}$  and  $a_w$  specified at 0.4, the warm pool temperature is roughly  $30^\circ$ . Here we describe a few properties of the solution that help to interpret the model sensitivity to increasing  $\text{CO}_2$ , described in the next section. The model behavior is similar to that of Pierrehumbert (1995), whose solutions are characterized by cold pool emissivity, analogous to our  $q_{\text{TL},c}$ , the specific humidity at the cold pool inversion.

Temperatures increase with  $q_{\text{TL},c}$  (Fig. 6a). This is because the cold pool longwave opacity increases with increasing upper-tropospheric moisture. If the total radiative flux emitted from the cold pool is to remain the same, the temperature of the cold pool upper troposphere must increase. Because of the vanishing horizontal temperature gradient above the Tropics and the joining of tropospheric temperatures over the warm pool to the surface by a moist adiabat, increased temperatures high above the cold pool require an increase in the warm pool surface temperature. This increases the net import of moist static energy into the cold pool so that the mixed layer of this region warms as well until the import is restored to near its original value.

At fixed  $q_{\text{TL},c}$ , both warm and cold pool temperatures increase with the size of the warm pool. This is because the total radiative gain by the warm pool increases as it expands. In order to compensate, OLR over the cold pool has to increase since the export of energy to mid-latitudes is fixed in this experiment. Again, this is brought about by an increase in the cold pool upper-tropospheric temperature, which leads to increases in the warm and cold pool surface temperatures. As  $q_{\text{TL},c}$  increases, the tropical temperature becomes less sensitive to the relative size of the two regions because the difference in opacity, and thus the differential radiative heating, becomes increasingly small.

#### 4. Low cloud cover and tropical sensitivity to doubled $\text{CO}_2$

In this section, we calculate whether low cloud cover amplifies or moderates the tropical response to climate forcing. We start with the equilibrium solution representing the present-day climate, shown in Fig. 6, and perturb it by doubling the  $\text{CO}_2$  concentration specified in the radiation model. In the equilibrium solution, low-cloud forcing is prescribed, along with forcing by deep convective clouds. In the sensitivity calculation below, perturbations in low cloud cover and forcing are calculated using empirical relationships derived by Klein and Hartmann (1993). Low cloud optical thickness is assumed to be fixed since it presumably depends in part upon cloud microphysics, which have a complicated and currently unclear relationship with the large-scale circulation computed by our model. In addition, convective cloud cover is held constant, since modeling the variability of these clouds requires a more sophisticated treatment of convection and cloud moisture than we wish to undertake.

Although at any instant low cloud cover depends upon a complicated interaction between cloud microphysics, radiation, and the large-scale circulation, an empirical formula accounting for a large percentage of variability of seasonal anomalies of stratus low cloud cover has been derived by Klein and Hartmann (1993). They relate variations in subtropical ISCCP stratus low cloud cover to variations in low-level static stability, according to

$$c' = 5.70\Delta\theta', \quad (30)$$

where  $c'$  is the anomalous stratus low cloud cover in percent and  $\Delta\theta'$  is the anomalous difference in potential temperature between 700 mb and the surface.<sup>2</sup> A similar parameterization has been proposed by Slingo (1980, 1987) for use in GCMs on the shorter timescale of a model integration time step. Since the surface potential temperature is nearly equal to SST, (30) is capable in principle of reproducing the observed negative correlation between SST and low cloud cover (e.g., Hanson 1991; Oreopoulos and Davies 1993; Norris and Leovy 1994), depending upon how  $\theta$  above the trade inversion changes in response to climate forcing.

Although (30) represents an empirical correlation, we assume (like the GCM studies cited above) that the relationship reflects a physical mechanism and is causal. This mechanism is possibly cloud-top entrainment instability (CTEI) (Randall 1980; Deardorff 1980), a process by which dry air subsiding through the trade inversion mixes with cloudy air at the cloud top. When the cloud is capped by a weak inversion, the evaporation of cloud liquid water can cool the mixture below the temperature of the cloudy air. The cold, negatively buoy-

<sup>2</sup> Potential temperature is calculated in the model according to  $\theta = T (P_0/P)^{R/C_p}$ , where  $P_0$  equals 1000 mb.

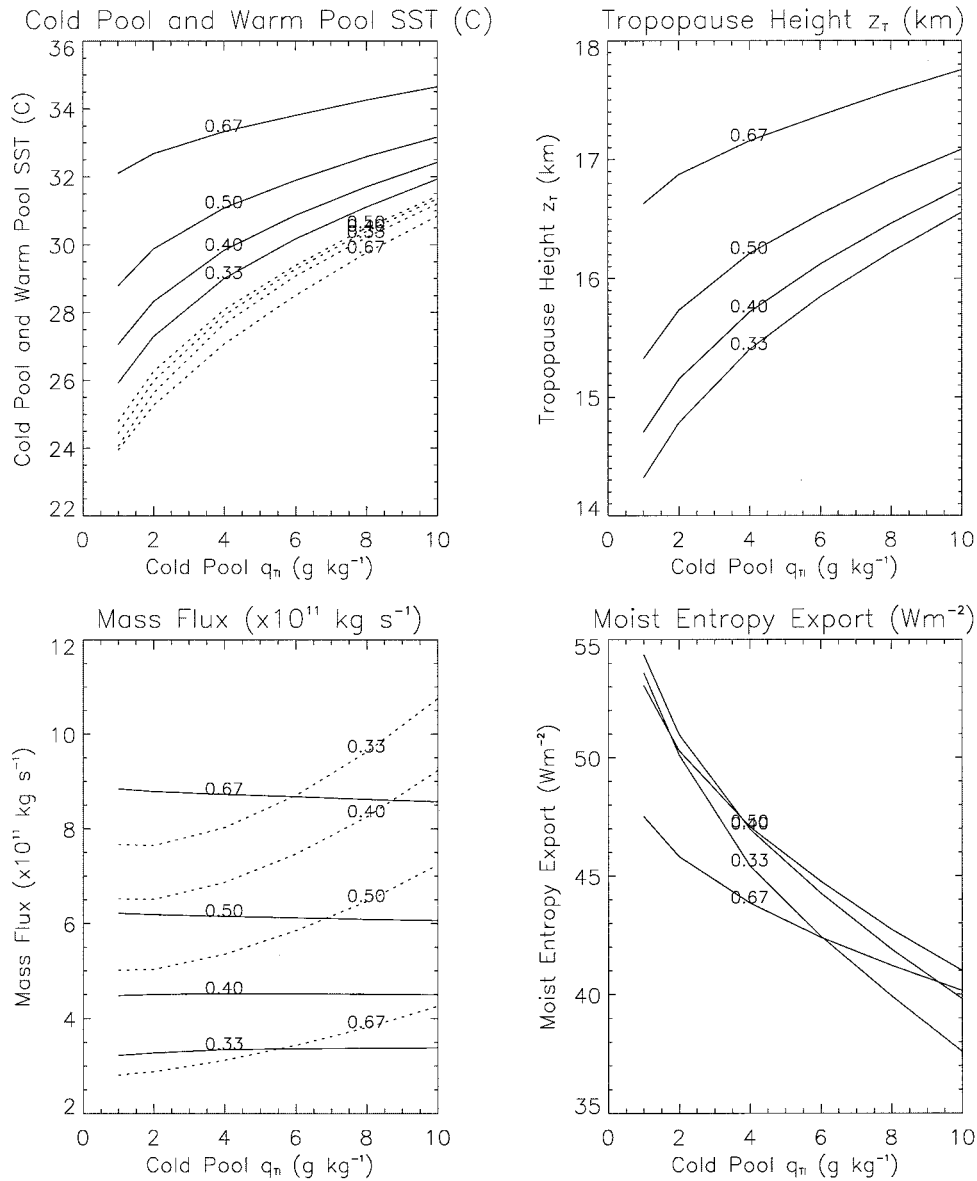


FIG. 6. Equilibrium solution given low cloud forcing of  $-15/a_w$   $\text{W m}^{-2}$  over the cold pool, convective cloud forcing of  $-7/a_w$   $\text{W m}^{-2}$  over the warm pool, and  $-5$   $\text{W m}^{-2}$  of uniformly distributed cooling. Warm pool solutions are denoted by solid lines, cold pool solutions are denoted by dashed lines. (a) SST ( $^{\circ}\text{C}$ ). (b) Tropopause height (km). (c) Area-integrated (dotted) pool mass fluxes—that is,  $M_w$  and  $M_c$  times the area of the warm and cold pools, respectively ( $\times 10^{11}$   $\text{kg s}^{-1}$ ). (d) Moist energy export from warm pool to cold pool. (e) Net radiative flux at the tropopause. (f) Net radiative flux at the surface. (g) Surface latent heat flux. (h) Surface sensible heat flux. (i) Mixed-layer specific humidity  $q_B$  ( $\text{g kg}^{-1}$ ). (j) Specific humidity at the trade inversion  $q_{TI}$  ( $\text{g kg}^{-1}$ ). (k) Detained hydrometeors at the tropopause  $l_{T,u}$  ( $\text{g kg}^{-1}$ ). (l) Tropically averaged precipitation ( $\text{mm day}^{-1}$ ).

ant mixture descends, evaporating additional water and eroding the cloud from within. In the presence of a sufficiently strong inversion, the mixture remains warm enough that it is unable to descend into the interior of the cloud. The “classic” criterion for CTEI (Randall 1980; Deardorff 1980), involving both the difference in temperature and moisture across the inversion at the cloud top, has not been found to accurately predict vari-

ations in low cloud cover at a single location at any given instant (e.g., Albrecht 1991). This is perhaps because the criterion does not reflect all the physical mechanisms that act to break up a stratus deck (e.g., Wang and Albrecht 1994). Another possibility is that an adjustment time must elapse before CTEI can change cloud cover in response to changes in the vertical profile of temperature and moisture. Changes in these prop-

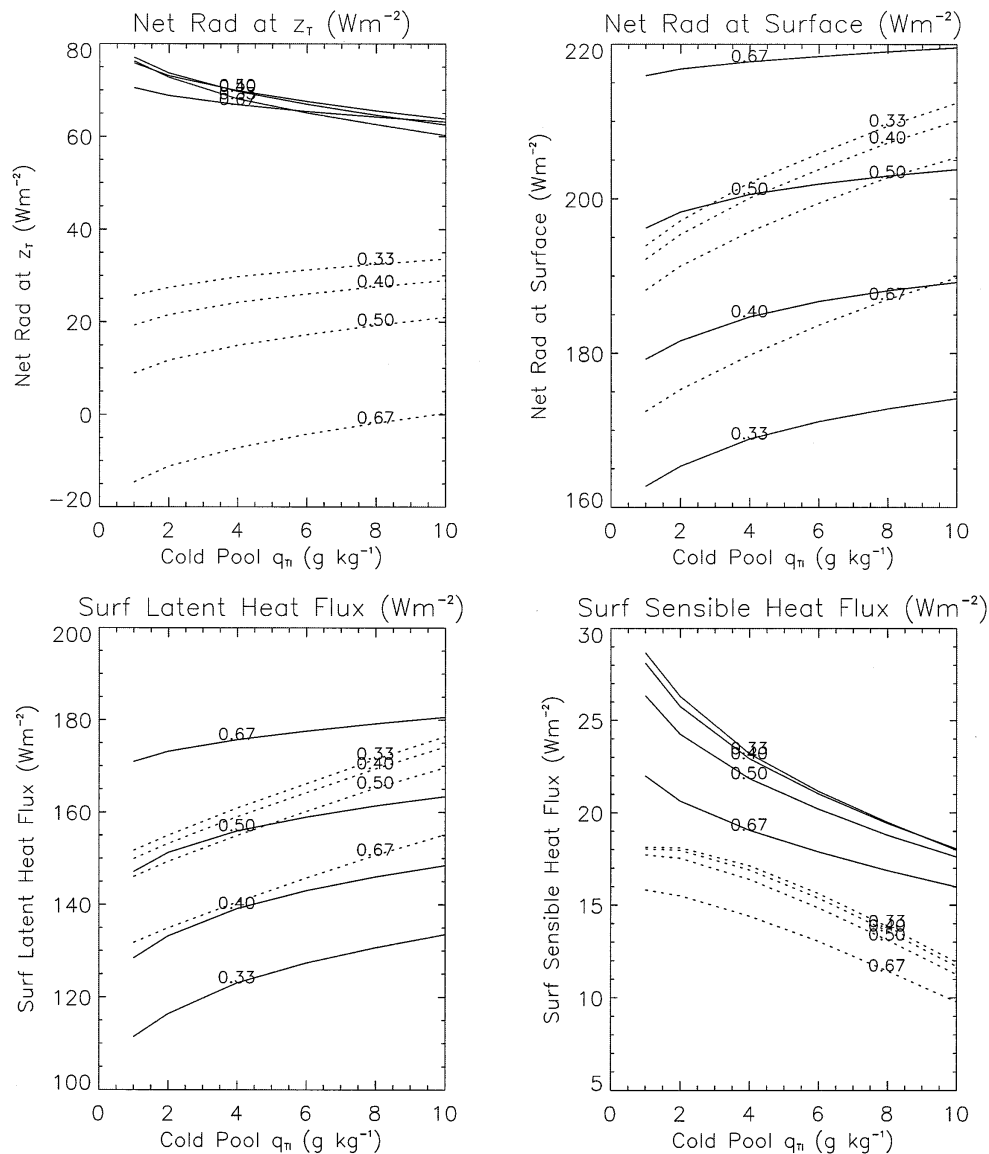


FIG. 6. (Continued)

erties upwind by as much as 24 hours might be a better predictor, according to the analyses of Klein et al. (1995), which also show that the CTEI criterion is significantly correlated with interannual variations in low-cloud amount on a longer (monthly) timescale. Whether CTEI is the physical basis for the empirical relation between static stability and low cloud cover found by Klein and Hartmann (1993) is currently unclear. It is also unclear why so much variability in cloud cover is accounted for by static stability alone, when the difference in moisture across the inversion is a fundamental part of the CTEI criterion. In any case, the relation (30) appears to account for a large fraction of seasonal variability in stratus low cloud cover over many different regions of the subtropics. It is also consistent with in-

terannual variations in cloud cover and static stability in the subtropical Pacific, where over two decades of observations exist (Klein and Hartmann 1993; Klein et al. 1995).

An empirical relation between variations in ISCCP stratus low cloud cover  $c'$  and anomalous ERBE TOA cloud forcing  $F'$  was also derived by Klein and Hartmann (1993):

$$F' = -1.162c', \quad (31)$$

where  $c'$  is in percent and  $F'$  is in  $W m^{-2}$ . As in the previous section, cloud forcing at all heights is assumed to be equal to the value at the top of the atmosphere. In appendix A, this assumption is examined using a mixing-line model to derive cloud properties, such as

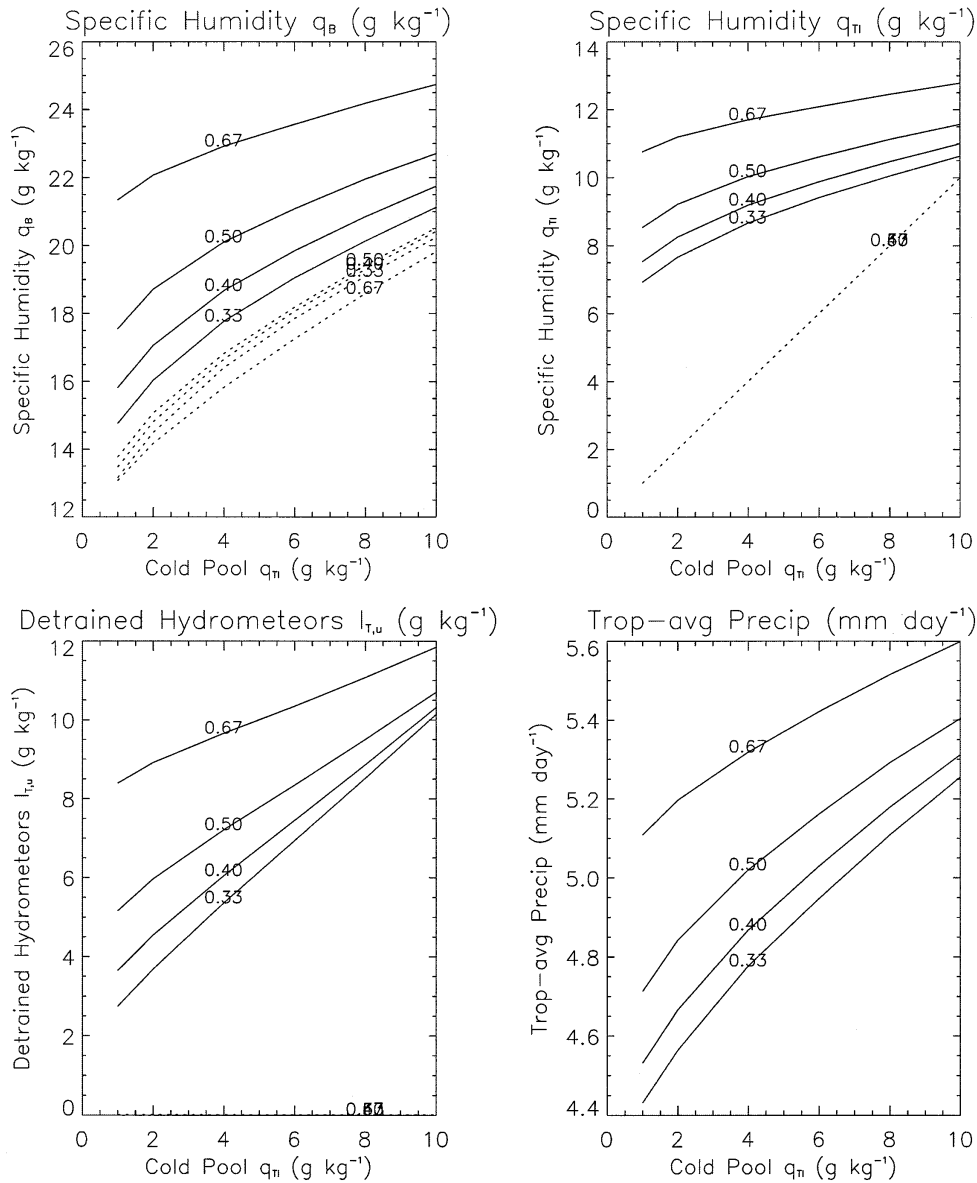


FIG. 6. (Continued)

temperature and liquid water content, in terms of properties of the large-scale circulation. The mixing-line model is based upon observations of marine stratocumulus clouds (Boers and Betts 1988) and reproduces the empirical relation between cloud cover and TOA cloud forcing derived by Klein and Hartmann (1993). Together with a radiative model, this allows the cloud forcing at all levels in the atmosphere to be calculated, rather than assumed equal to the TOA value. Despite the differences in complexity, we find that the two approaches give essentially the same climate sensitivity as a function of low cloud cover.

Before presenting the results of the sensitivity calculation, we note that as a consequence of (30) and (31), the sensitivity of stratus low-cloud forcing to

changes in low-level static stability is  $6.62 \text{ W m}^{-2}$  per  $^{\circ}\text{C}$ . Compared to the  $4 \text{ W m}^{-2}$  associated with doubled  $\text{CO}_2$ , this is a potentially strong feedback for changes in stability as small as a few tenths of a degree, at least in regions like the subtropics where the circulation favors low-cloud formation. However, while we expect SST to increase by a few degrees as  $\text{CO}_2$  increases, the magnitude and sign of the change in stability are less clear a priori.

Figure 7a shows the change in SST in response to doubled  $\text{CO}_2$ , with  $a_w$  set equal to 0.4. (Nearly identical results were found with  $a_w$  set equal to 0.33 and 0.5.) The perturbed tropical climate is calculated assuming that the moisture content above the cold pool inversion is unchanged. While on interannual timescales temper-

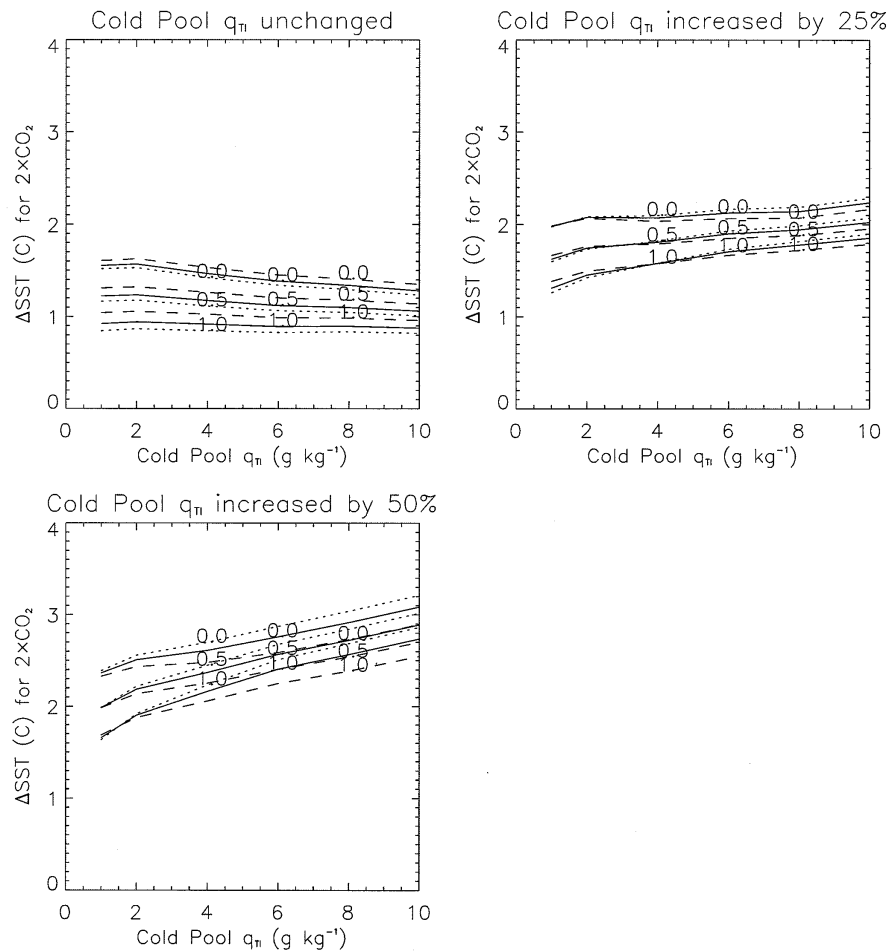


FIG. 7. Changes in SST in response to doubled CO<sub>2</sub> for the warm pool (dashed), cold pool (dotted), and tropical average (solid). The experiment with fixed cloud cover is denoted by 0.0, the experiment where forcing by low cloud cover responds to the perturbed model state is denoted by 1.0, and the experiment where low cloud cover sensitivity to cold pool static stability is reduced by one-half is denoted by 0.5. In response to doubled CO<sub>2</sub> specific humidity at the cold pool inversion is assumed (a) constant, (b) to increase by 25%, and (c) to increase by 50%.

atures above the boundary layer vary in unison across the entire Tropics, moisture variations seem confined to within the convecting region (Sun and Oort 1995). In addition, Chou (1994a) has used ERBE TOA radiative fluxes to infer that the subtropics became increasingly dry during the 1987 ENSO event, despite tropicwide warming and increased convection. Subtropical drying in response to increased convection in the deep Tropics was also inferred by Bates et al. (1996), based upon over a decade of satellite measurements of longwave emission. It is unclear whether these variations are proxies for the changes in cold pool moisture forced by the doubling of CO<sub>2</sub>, and we present additional sensitivity calculations below in which  $q_{TL,c}$  is increased.

There are three sets of curves in Fig. 7a, each set consisting of the change in warm pool (dashed), cold pool (dotted), and tropically averaged (solid) temperature. The set denoted “0.0” shows the change in tem-

perature for the control experiment, wherein low-cloud forcing is held fixed. In the experiment denoted “1.0,” perturbations to low-cloud forcing are computed using (30) and (31). The set of curves labeled “0.5” corresponds to an identical experiment except that static stability in the relation (30) is multiplied by a factor of 1/2. This is to include the possibility that the empirical relation between stratus cloud cover and static stability is not universal but perhaps depends upon the horizontal scale over which variations are averaged prior to the regression calculation. [Of course it is possible that cloud cover is an even stronger function of static stability than indicated by (30).] The difference in  $\Delta$ SST between the three sets of curves is a measure of the strength of the low cloud cover feedback. As a result of reducing the sensitivity of low cloud cover to static stability by a factor of 0.5, the low-cloud feedback is correspondingly reduced by roughly one-half, and we

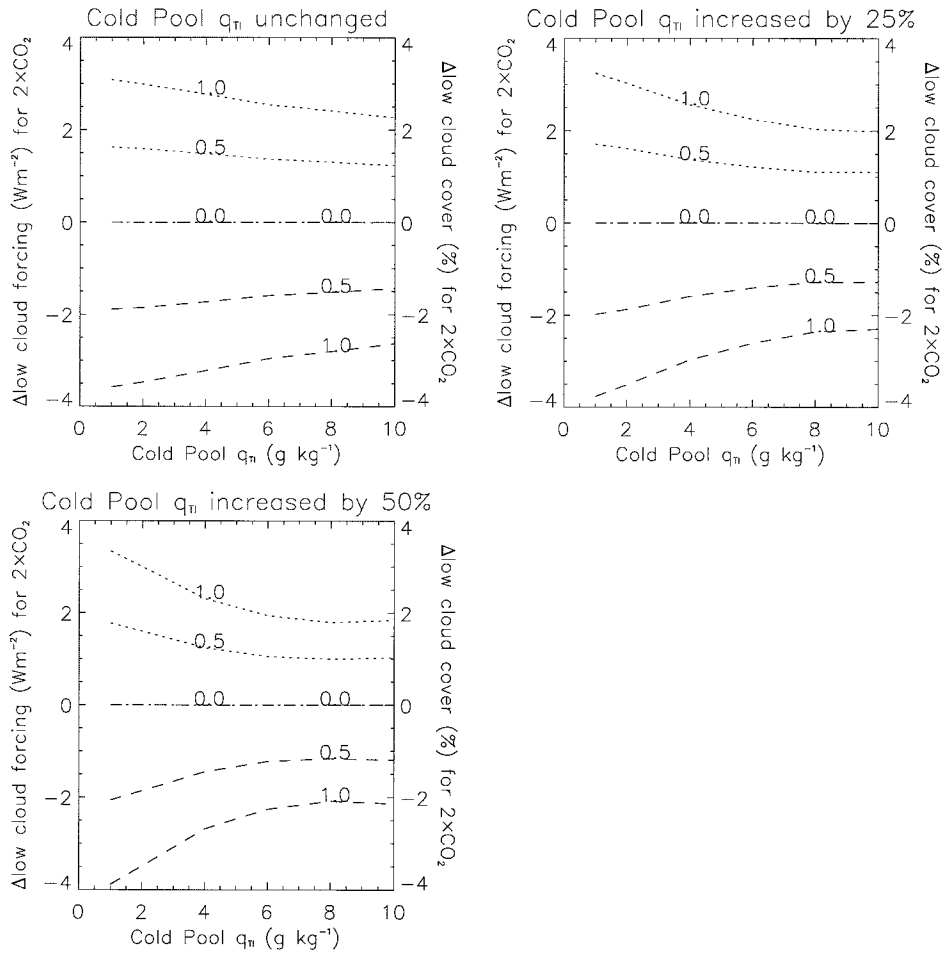


FIG. 8. As in Fig. 7 except for low cloud cover (dotted, %) and forcing (dashed,  $\text{W m}^{-2}$ ) over the cold pool. A 1% change in cloud cover over the cold pool is equivalent to a 0.6% change in the tropical average for  $a_w = 0.4$  and  $a_c = 0.6$ .

will not comment further upon this particular experiment.

The most noteworthy feature of the low cloud cover feedback is that it is negative. Whereas for fixed cloud forcing, tropical SST increases by roughly a degree and a half in response to doubled  $\text{CO}_2$ , this increase is reduced by a third to just under one degree when low cloud cover is allowed to respond to the changing circulation. This is the opposite of the positive low-cloud feedback that might be inferred based upon the observed negative correlation between SST and low cloud cover (e.g., Hanson 1991; Oreopoulos and Davies 1993). This positive feedback is permitted in principle by our model since cloud cover varies with SST through (31). Increases in the cold pool 700-mb potential temperature are larger than warming at the surface, however, so that the low-level stability increases as well, causing an increase in low cloud cover and negative cloud forcing despite the increase in SST (Fig. 8a). We will return to the question of why static stability increases.

The change in cloud forcing is roughly  $3 \text{ W m}^{-2}$  (Fig.

8a), comparable to the  $4 \text{ W m}^{-2}$  forcing associated with doubled  $\text{CO}_2$ . The reason the change in SST is not nearly zero despite this near compensation is that there are other feedbacks in the model. For example, as the warm pool temperature increases, so does the moisture above the warm pool inversion. This is the clear-sky greenhouse effect, representing a positive feedback. Our model possibly overestimates the size of this feedback since although tropically averaged moisture is observed to increase in response to interannual variations in surface temperature, this increase is overestimated by the assumption of a constant relative humidity profile (Sun and Oort 1995). If interannual variability is a proxy for climate change, then our model, which fixes relative humidity over the warm pool, may overestimate the clear-sky greenhouse effect.

A  $3 \text{ W m}^{-2}$  low cloud cover feedback is equivalent to roughly a one-half degree increase in static stability. Because the large-scale circulation maintains a nearly uniform horizontal distribution of tropical temperature above the trade inversion (Sun and Oort 1995), while

convection relates the vertical distribution of temperature above the warm pool to the surface value (Betts 1982; Xu and Emanuel 1989), potential temperature above the cold pool inversion varies with the warm pool surface temperature. Thus, we can write

$$\begin{aligned}\Delta\theta &= \theta_{700\text{mb},c} - T_{s,c} \\ &= (T_{s,w} - T_{s,c}) + \Delta\theta_{w,ma},\end{aligned}\quad (32)$$

where  $\Delta\theta_{w,ma}$  is a measure of the warm pool low-level static stability, equal to the increase in potential temperature along a moist adiabat between the surface and 700 mb. Consequently, cold pool static stability and low cloud cover depend upon the difference in warm pool and cold pool surface temperatures, along with static stability over the warm pool. Figure 7a shows that the difference in warm and cold pool temperature is increased by 0.1 K in the absence of low-cloud feedbacks and by roughly twice this amount when cloud feedbacks are included. (The reason for this increase is examined in appendix B.) Roughly half of the increase in cold pool static stability associated with doubled  $\text{CO}_2$  results from the increased temperature difference between the warm and cold pools, with the remainder coming from the increase in warm pool low-level static stability. As the warm pool surface temperature increases, greater mixed-layer humidity leads to greater condensation heating and warmer potential temperatures aloft.

This sensitivity calculation has been carried out assuming that cold pool upper-tropospheric moisture is fixed. Increased cold pool moisture would reduce the radiative contrast between the warm and cold pool, perhaps reducing the surface temperature difference and the low cloud cover feedback. Upper-tropospheric moisture is indeed expected to change in response to doubling  $\text{CO}_2$ , although the magnitude of this change, and even the sign, are debated (e.g., Lindzen 1990; Betts 1990). Moisture over the cold pool inversion is not predicted by our model since this presumably requires a complicated estimate of the number of hydrometeors detraining from deep convective clouds (Sun and Lindzen 1993a) along with a model of horizontal mixing by transient eddies (Yang and Pierrehumbert 1994). However, we can impose a greater amount of moisture upon the perturbed climate by subtracting a present-day model solution from a solution computed assuming doubled  $\text{CO}_2$  along with a larger value of  $q_{\text{TL},c}$ .

Figures 7b,c show the increase in SST corresponding to doubling  $\text{CO}_2$ , assuming that specific humidity at the cold pool inversion increases by 25% and 50%, respectively. The warming is plotted as a function of the present-day (i.e., unperturbed) cold pool moisture. Low cloud cover feedbacks continue to reduce by roughly one-half degree the warming associated with doubled  $\text{CO}_2$ , despite an increase in cold pool moisture. Because detrained hydrometeors supply upper-tropospheric moisture over both the warm and cold pools, one estimate of the change in cold pool moisture is provided

by the warm pool moisture perturbation. The perturbation to  $q_{\text{TL},w}$  is shown in Figs. 9a–c. Given that the unperturbed values of  $q_{\text{TL},w}$  lie in the range of 8 to 10  $\text{g kg}^{-1}$  (Fig. 6j), we see that the warm pool moisture content never rises above roughly 25% of its unperturbed value so that an increase of cold pool humidity in the upper troposphere by 50% is probably a generous upper bound of the anticipated change.

The warming of the Tropics can be decomposed into two contributions,

$$\frac{\delta T}{\delta \text{CO}_2} \approx \left. \frac{\partial T}{\partial \text{CO}_2} \right|_{q_{\text{TL},c}} + \left. \frac{\partial T}{\partial q_{\text{TL},c}} \right|_{\text{CO}_2} \frac{\delta q_{\text{TL},c}}{\delta \text{CO}_2}. \quad (33)$$

The first term on the right-hand side represents the warming due to doubling  $\text{CO}_2$  at constant  $q_{\text{TL},c}$ . This effect is illustrated in Fig. 7a. The second term is proportional to

$$\left. \frac{\partial T}{\partial q_{\text{TL},c}} \right|_{\text{CO}_2},$$

the change in temperature with  $q_{\text{TL},c}$ , computed assuming a fixed concentration of  $\text{CO}_2$ . This effect is illustrated in Fig. 6a and corresponds to the clear-sky greenhouse effect. As  $q_{\text{TL},c}$  increases, the moisture profiles and corresponding radiative fluxes of the warm and cold pools become increasingly similar so that the equilibrium temperatures approach each other as well. Consequently, if as a result of doubling  $\text{CO}_2$  the cold pool upper-tropospheric moisture increases, the difference between the warm and cold pool surface temperature decreases. [Compare Fig. 7a, where  $\delta(T_{s,w} - T_{s,c}) > 0$ , to Figs. 7b,c, where  $\delta(T_{s,w} - T_{s,c}) < 0$ .] A decrease in the surface temperature contrast between the warm and cold pools would by itself reduce low cloud cover. However, this effect upon cold pool static stability is more than offset by the change in the warm pool temperature profile to a warmer moist adiabat, causing  $\Delta\theta_{w,ma}$  to increase as well. Figures 7b,c show that whether the cold pool moisture is increased by 25% or by 50%, low cloud cover feedbacks reduce the warming by roughly one-half a degree, despite the increased warming of the cold pool.

The low cloud cover feedback is negative in our model and reduces the warming associated with doubled  $\text{CO}_2$  by roughly a third. This reduction is calculated in the absence of feedbacks involving upper-tropospheric moisture over the cold pool. The low-cloud feedback continues to moderate tropical warming even when cold pool moisture is increased. This is because  $\Delta\theta_{w,ma}$ , the potential temperature difference along the warm pool adiabat between the surface and 700 mb, increases as the underlying mixed layer warms. Low cloud cover depends additionally upon  $(T_{s,w} - T_{s,c})$ , the difference in surface temperature between the warm and cold pools. Whether this difference increases or decreases is strongly dependent upon the relative change in upper-tropospheric moisture between the warm and cold pools. Although the subtropical upper troposphere seems to

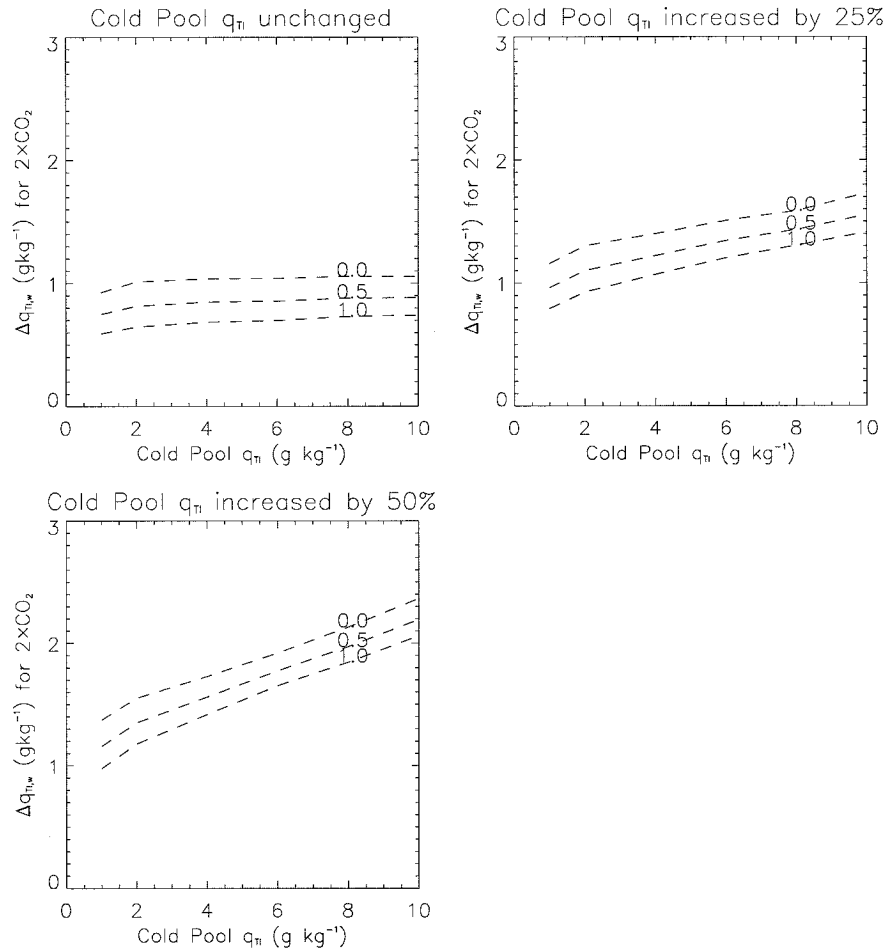


FIG. 9. As in Fig. 7 except for  $q_{T_w}$ , the specific humidity at the warm pool trade inversion.

dry out in response to interannual variations in SST when convection is strengthened (Chou 1994b; Bates et al. 1996), it is not clear whether this variability is a proxy for the changes in moisture forced by rising concentrations of  $\text{CO}_2$ . The more general point is that since low cloud cover reflects the thermodynamic properties of the surface along with those of air subsiding through the inversion, the low-cloud feedback will depend upon the entire tropical circulation and cannot be inferred simply from local correlations with SST.

## 5. Conclusions

The aim of this study has been to examine the response of subtropical stratus low cloud cover to climate perturbations in the context of the entire tropical circulation. Stratus low cloud cover is empirically related to the difference between potential temperature above the trade inversion (at 700 mb) and the surface. The Hadley and Walker circulations maintain horizontally uniform temperatures above the boundary layer, and the vertical profile of temperature within convecting regions is related to the surface properties by moist convection.

Consequently, variations in the subtropical 700-mb potential temperature are related to variations in the surface layer of the convecting region so that stratus low cloud cover depends upon distant convecting regions in addition to the underlying SST.

We have constructed a simple model of the tropical climate in order to estimate how stratus low cloud cover might respond to changes in the circulation forced by increasing  $\text{CO}_2$ . The model consists of a warm pool in which convective updrafts are embedded and a cold pool over which air descends before rejoining the trades that feed the updrafts. The cold pool is the locus of stratus low clouds in the model. Budgets of dry static energy and moisture are constructed, and the effects of dynamics are treated implicitly by assuming that the large-scale circulation maintains horizontally uniform temperatures above the trade inversion. The model is simplified by using the fact that the updraft extent is small compared to the area of the descending regions—on the order of a few percent according to observations of deep convective cloud cover by ISCCP. In the limit of vanishing updraft extent, thermodynamic properties at the

tropopause and the warm pool surface are connected by a moist adiabat.

We estimate the feedback associated with stratus low cloud cover by perturbing the model with doubled  $\text{CO}_2$ . Changes in stratus low cloud cover and cloud radiative forcing are estimated from the cold pool low-level static stability calculated by the model, using the empirical relations derived by Klein and Hartmann (1993). The cloud radiative forcing is assumed to be independent of height, although we show in appendix A that a more elaborate calculation of this forcing leads to the same conclusions about the importance of the stratus low cloud cover feedback.

Stratus low cloud cover is found to be a negative feedback, increasing in response to doubled  $\text{CO}_2$  and reducing the tropically averaged warming by one-third, compared to the warming with low cloud cover held fixed. Although located within the cold pool, low clouds can moderate warm pool temperatures through the large-scale circulation since a reduction in moist static energy within the cold pool mixed layer increases the net export of moist static energy out of the warm pool. The increase in low cloud cover is associated with an increase in low-level static stability over the cold pool. This stability is related to the warm pool low-level static stability  $\Delta\theta_{ma}$  (equal to the change in potential temperature between the surface and 700 mb along the warm pool moist adiabat), as well as the difference in surface temperature between the warm and cold pools [cf. (32)]. As the warm pool surface temperature rises, the change in potential temperature along a moist adiabat rises due to the increased moisture at the surface. The difference in surface temperature also increases with  $\text{CO}_2$ . In appendix B, this is shown to result from the increased radiative gain within the warm pool as  $\text{CO}_2$  increases and the need to compensate by increasing the export of moist static energy through a strengthening of the horizontal gradient of this quantity.

Upper-tropospheric moisture over the cold pool is held fixed in the above calculations. On an interannual timescale, it decreases as convection within the deep Tropics increases (Bates et al. 1996), although it is unclear whether this drying will occur as the concentration of  $\text{CO}_2$  rises. The difference in warm and cold pool surface temperature is very sensitive to cold pool upper-tropospheric moisture, and to measure the sensitivity of the low-cloud feedback, we computed the response to doubled  $\text{CO}_2$  assuming that moisture in this region increases. For sufficient moistening, the difference in the warm and cold pool surface temperature anomaly is reversed. Nonetheless, stratus low cloud cover remains a negative feedback due to the increase in warm pool low-level static stability.

Our result that low cloud cover represents a negative feedback to tropical climate is in contrast to the positive feedback that might be inferred from the observed negative correlation between low cloud cover and SST (e.g., Hanson 1991; Oreopoulos and Davies 1993). Note that

our model has the potential for a positive feedback since perturbed cloud cover is proportional to anomalous low-level static stability and thus could be negatively correlated with variations in SST. Although SST rises in our model in response to doubling  $\text{CO}_2$ , the potential temperature at 700 mb increases by more, so that the anomalous low-level static stability is positive, resulting in an increase in low cloud cover.

Our model is essentially an idealized version of the Hadley–Walker circulation, and many processes have been omitted. For example, we assume that the lapse rate above the trade inversion is moist adiabatic, even though our model requires only that the mixed layer and tropopause values be connected by a moist adiabat. This assumption affects our estimate of the warm pool low-level static stability  $\Delta\theta_{ma}$ . We could compute the lapse rate with greater precision and vertical resolution by dividing the troposphere into more than two layers and computing budgets of dry static energy for each. However, note that an accurate determination of the lapse rate requires precise knowledge of the distribution of upper-tropospheric water vapor (Sun and Lindzen 1993b) so that the radiative cooling can be calculated accurately, along with knowledge of the vertical distribution of the mass flux. The mass flux is strongly dependent upon the cumulus parameterization. Neither the change in upper-tropospheric water vapor nor the vertical dependence of the mass flux in response to increasing  $\text{CO}_2$  can be confidently predicted at the moment.

The model response to doubled  $\text{CO}_2$  has been computed assuming that the export of moist static energy to the midlatitudes by atmospheric eddies and ocean transports is unchanged. Using a coupled GCM, Manabe and Stouffer (1993) find that the total poleward energy flux out of the Tropics is relatively insensitive to changes in  $\text{CO}_2$ , although the partitioning of this flux between ocean and atmospheric latent and sensible heating does vary. Midlatitude eddies can also influence subtropical cloud cover by modulating temperature above the cloud-top inversion. Klein et al. (1995) note that during the NH summer, large stratus cloud cover in the subtropical Pacific is associated with steady cold advection within the surface layer. This steady flow is disrupted by midlatitude eddies traveling along the neighboring storm track. Changes in storm frequency, intensity, or in the storm tracks themselves as a result of increasing  $\text{CO}_2$  might alter the subtropical low-cloud amount.

In addition, our model omits changes in low-cloud forcing related to optical thickness. Treatment of this effect requires a careful treatment of cloud microphysics, including an estimate of how CCN concentrations will change in response to climate forcing. In appendix A, we note that the radiative forcing associated with marine stratus clouds is sensitive to small changes in cloud thickness, which alters the cloud optical thickness. Although variations in cloud cover rather than optical thickness account for most of the observed variation in

stratus-cloud forcing (Klein and Hartmann 1993), this empirical relation is based upon seasonal changes and optical thickness may play a comparatively larger role in the response to increasing greenhouse gases. Clearly, parameterizations of low-cloud optical thickness in addition to cloud cover are needed. The goal of this study has been to infer the feedback when low cloud cover is allowed to vary with static stability rather than simply with SST. It is hoped that through experimental programs like ASTEX (e.g., Albrecht et al. 1995) an improved theoretical understanding of subtropical low clouds can be achieved and that this will lead to more complete parameterizations. Note that such parameterizations can be incorporated into our simple tropical model in order to study interactions of low clouds with the remainder of the tropical climate, as a relatively simple alternative to a full atmospheric GCM.

Our model computes changes in cloud forcing only by subtropical stratus. Changes in trade cumulus amount along with changes in low-cloud amount in the convecting region are neglected. Covariability between these cloud types and subtropical stratus low clouds is being investigated using the ISCCP dataset. Again, note that stratus low cloud cover by itself accounts for a large fraction of variability in subtropical cloud forcing (Klein and Hartmann 1993).

Perhaps the biggest limitation of a model such as this is that the areal extent of the warm and cold pools is prescribed (Pierrehumbert 1995). To be sure, the size of the convecting region does not seem to change appreciably throughout the year, despite large changes in the location of deep convection (Table 1). We suggest one mechanism by which  $a_w$  is possibly controlled, which is being investigated. By continuity, the mass flux  $a_c M_c$  associated with subsidence over the cold pool must equal the horizontal flux from the cold pool mixed layer into the warm pool. This horizontal flux must also be consistent with the pressure gradient within the surface layer, a dynamical constraint that is absent in our model. This pressure difference can be related to the temperature difference within the boundary layer using the hydrostatic relation (e.g., Schneider 1977; Lindzen and Nigam 1987) since temperature is horizontally uniform above the inversion. Thus, the mass flux corresponding to cold pool subsidence must be consistent with the temperature difference between the warm and cold pools. Since the subsidence rate  $M_c$  is determined by the rate of radiative cooling, the only way for the subsiding air to adjust its associated mass flux to the surface temperature difference is to adjust the horizontal area of the descending branch—that is, the horizontal area of the cold pool.

Since according to this mechanism the cold pool area is related to the temperature difference between the warm and cold pools, low cloud cover will be sensitive to changes in the areal extent of each region. This emphasizes again that tropical low cloud cover depends

upon the entire tropical circulation and not just local processes that can be expressed by a local correlation.

*Acknowledgments.* This work was inspired by discussions with the Tropical SST Regulation Reading Group, led by Richard Seager at the Lamont-Doherty Earth Observatory. Andy Lacis, Makiko Sato, and Barbara Carlson generously provided the GISS radiation code and instruction in its use. The presentation of this article was greatly improved by the comments of two anonymous reviewers. The author is also grateful to Brian Cairns, Stephen Klein, David Neelin, Ray Pierrehumbert, William Rossow, Qingqiu Shao, and especially Anthony Del Genio for illuminating conversations about the tropical atmosphere. This work was supported by the First ISCCP Regional Experiment and the National Science Foundation through Grant ATM-94-22631 of the Climate Dynamics Division.

#### APPENDIX A

##### Low Cloud Cover Feedbacks with an Alternative Cloud Radiation Model

Given stratus low cloud cover, TOA cloud forcing has been computed using the empirical relation derived by Klein and Hartmann (1993). For simplicity, we have assumed that low-cloud forcing at other levels is identical to the TOA value. This idealization is useful because cloud longwave forcing and cloud absorption of solar radiation have small and offsetting effects upon the divergence of the net flux between the surface and the top of the atmosphere (Norris and Leovy 1994). In this appendix, we examine whether our conclusions regarding the low cloud cover feedback are robust by carrying out a more careful estimation of cloud radiative forcing as a function of height. The cold pool is divided into cloudy and clear-sky regions, and the radiative fluxes from each are combined to form the area-averaged cold pool flux

$$R_c(z) = (1 - c_f)R_{c,\text{clear}}(z) + c_f R_{c,\text{cloudy}}(z),$$

where  $c_f$  is the fractional cloudiness within the cold pool. The radiative model requires the specification of temperature and moisture within both regions, along with cloud optical thickness. Thermodynamic properties of the clear-sky and cloudy regions are assumed to be identical beneath the lifting condensation level and above the trade inversion. Between these two levels, a mixing-line model is used to compute temperature and moisture within the clear-sky region, as in previous sections. A mixing-line model is also used to compute temperature and moisture within the cloudy region, along with cloud optical thickness, as described below. This allows the cloud forcing to be computed explicitly at all levels throughout the troposphere. We find that the low cloud cover feedback to increasing CO<sub>2</sub> is virtually unchanged despite the more elaborate calculation of cloud forcing.

The advantage of our approach is that cloud forcing at any level can be calculated rather than assumed identical to the TOA value, obviating the need for the approximations described above. The disadvantage is that we have to make alternative simplifying assumptions about the cloud properties. In particular, we assume that subtropical stratus clouds can be represented by a single cloud type. While the calculation described in this section introduces its own drawbacks, it is useful as an additional “reasonable” method of estimating cloud forcing and can be used to measure the robustness of our conclusions described in the previous section.

A mixing-line cloud model is based upon the observation that thermodynamic properties of air within subtropical clouds reflect to a good approximation conservative mixing of air between the mixed layer and air subsiding through the inversion (Betts 1982; Betts and Ridgway 1989). The model requires the specification of cloud height and the parameter  $\beta \equiv dp^*/dp$ . This parameter measures how rapidly the pressure  $p^*$  of the mixture’s saturation level varies with the actual pressure  $p$ . Since the air is just saturated at cloud base (so that  $p^*$  is equal to  $p$ ),  $\beta$  less than unity means that, at all levels above, the saturation level lies below the mixture, so that the mixture contains liquid water that has condensed. Boers and Betts (1988) suggest that  $\beta = 0.4$  is a typical value for marine stratus clouds above cloud base. That trade cumuli are represented by  $\beta = 0.6$  (Betts and Albrecht 1987) suggests that this parameter does not vary much across the spectrum of subtropical cloud types.

Estimating a representative cloud height is more difficult since marine stratus clouds can range in thickness from a few hundred meters near the upwind eastern edge of the subtropics to a kilometer or more in the region of transition to trade cumulus. In fact, within the transition region, individual cumulus towers are a kilometer thick with a thinner stratus layer near their top (e.g., Albrecht et al. 1995). It is impossible for a single cloud type to represent this range of morphology. We will simply assume that cloud top lies at 1100 m above the surface, with the top of the inversion (denoted by  $z_{TL,c}$  in Table 2) at 100 m above. Since the lifting condensation level over the cold pool is near 600 m, this results in a cloud thickness of 500 m and cloud liquid water mixing ratio  $l$ , rising from zero at cloud base to near  $0.4 \text{ g kg}^{-1}$  just below cloud top (where  $l$  falls to zero by definition). These are reasonable values (e.g., Albrecht et al. 1988; Wang and Rossow 1995) and give cloud optical thicknesses that are roughly in agreement with those needed to reproduce the ERBE low-cloud forcing at the TOA.

Cloud optical thickness  $\tau(z)$  within a cloud layer of depth  $\Delta z$  is related to liquid water mixing ratio  $l$  according to

$$\tau(z) = \frac{3 l \rho_{\text{air}} \Delta z}{2 \rho_w r_e}, \quad (34)$$

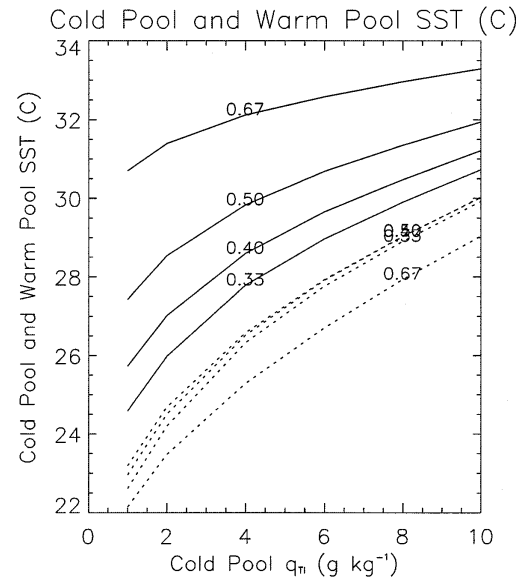


FIG. 10. Warm pool (solid) and cold pool (dotted) SST, given observed energy export to the midlatitudes by atmospheric eddies and ocean transports. Each curve represents a different value of the fractional area corresponding to the warm pool. Low cloud cover of 20% is specified over the cold pool, with low-cloud radiative forcing calculated using a cloud mixing-line and radiative model, along with prescribed total cloud optical thickness. Convective cloud forcing of  $-7/a_w \text{ W m}^{-2}$  is prescribed over the warm pool.

where  $\rho_{\text{air}}$  and  $\rho_w$  are the densities of air and water, respectively, and  $r_e$  is approximately the radius of the cloud droplets (Stephens 1978). For values of liquid water characterizing our model clouds, Del Genio et al. (1995) assume that  $r_e$  increases as the one-third power of  $l$ . We will compute the vertical dependence of cloud optical thickness according to (34). Note that the goal of this study is to estimate the low cloud cover feedback to increasing  $\text{CO}_2$ , as distinguished from the feedback due to low-cloud optical thickness. While cloud optical thickness as a function of height is needed to compute cloud radiative forcing, we will remove the cloud optical thickness *feedback* by rescaling  $\tau(z)$  so that the total cloud optical thickness, equal to the sum of  $\tau(z)$  at all cloud levels, is identical in all cases.

Using the mixing-line cloud model along with the radiation model to compute cloud forcing, we recomputed the present-day tropical climate, assuming a total cloud optical thickness of 9. The resulting SST is shown in Fig. 10, while Fig. 3 displays vertical profiles of temperature, specific humidity, and cloud liquid water for the case of  $q_{TL,c}$  equal to  $5 \text{ g kg}^{-1}$  and  $a_w$  equal to 0.4. Normalized cloud forcing at the tropopause, the top of the mixed layer, and the surface are shown in Figs. 11a–c, which depict  $R_{c,\text{cloudy}} - R_{c,\text{clear}}$ , the difference between the cloudy and clear-sky fluxes over the cold pool. (Since cloud forcing  $F$  is defined as the difference between the total and clear-sky fluxes,  $R_{c,\text{cloudy}} - R_{c,\text{clear}}$  is equal to the cloud forcing divided by  $c_p$ , the cold pool

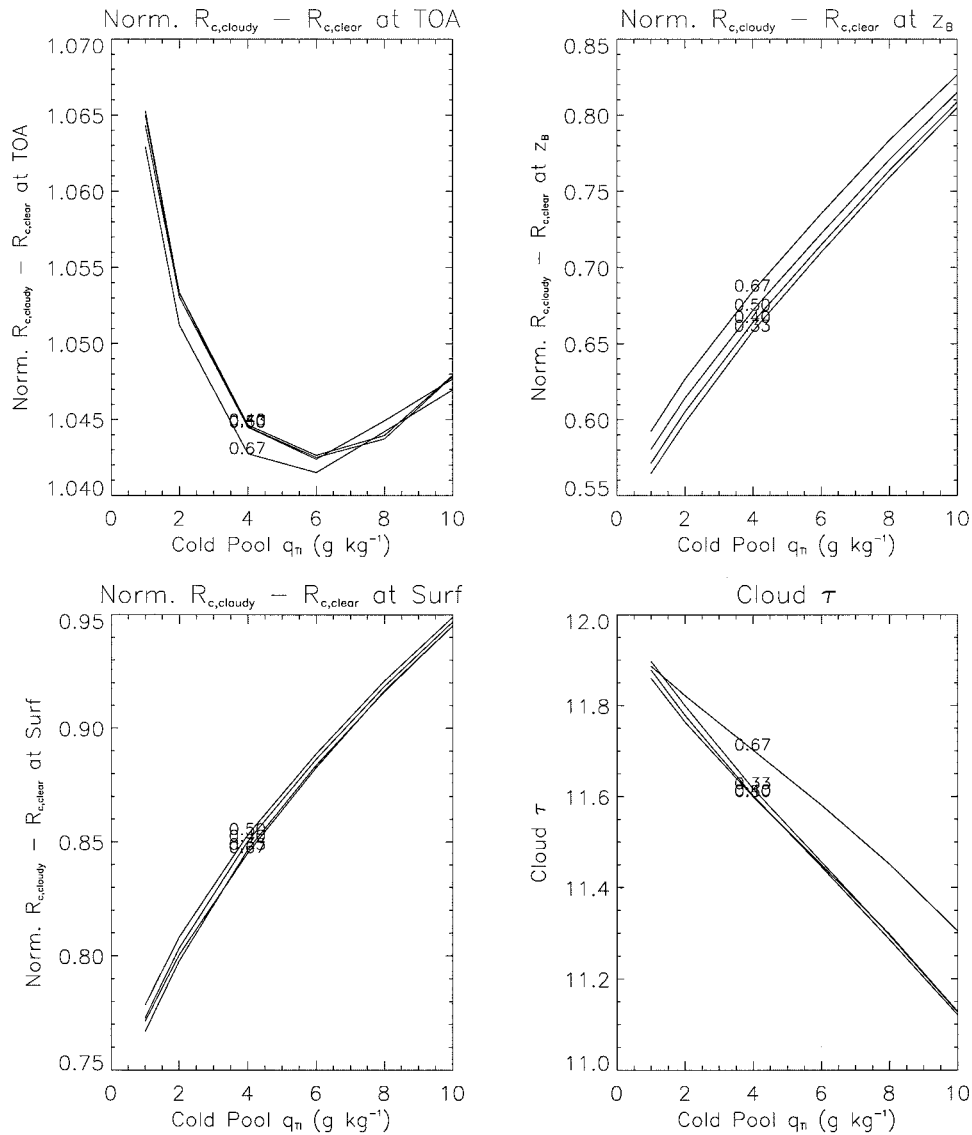


FIG. 11. As in Fig. 10 except that normalized cloud radiative forcing at the tropopause, top of the mixed layer, and surface are shown, along with cloud optical thickness computed from the cloud liquid water. (Note that this value of cloud optical thickness is not used in the radiative calculation.)

fractional cloudiness.) For comparison,  $R_{c,cloudy} - R_{c,clear}$  in Figs. 11a–c has been normalized by the observed TOA value of  $-1.162 \text{ W m}^{-2}$  percent $^{-1}$  estimated by Klein and Hartmann (1993) from ERBE measurements. Thus, a value of unity in Fig. 11a represents perfect agreement with ERBE. In fact, the model TOA value is nearly unity, in agreement with ERBE over a large range of  $q_{TL,c}$  and  $a_w$ .

Normalized cloud forcing at the top of the mixed layer and at the surface are shown in Figs. 11b,c, respectively. To the extent that cloud forcing is independent of height, as assumed in the previous sections, these normalized forcings should be equal to unity. This is seen to be only approximately true. The assumption of constant cloud forcing with respect to height results in an over-

estimation of cloud forcing at both these levels, causing exaggerated cooling of the surface and an underestimation of radiative cooling and the associated rate of descent above the surface layer.

The solution in Figs. 10 and 11 was calculated assuming TOA convective cloud forcing of  $(-7/a_w) \text{ W m}^{-2}$  within the warm pool and correspondingly decreased radiative divergence in the overlying troposphere, as assumed in the previous sections. Rather than cool the model with the observed ERBE low-cloud forcing, this time we specified the annual average tropical low cloud cover at 20% [so that  $c_f$  is equal to  $(0.20/a_c)$ ], consistent with ISCCP, and computed the associated cloud forcing explicitly using the mixing-line cloud model described above. Observed ISCCP annually av-

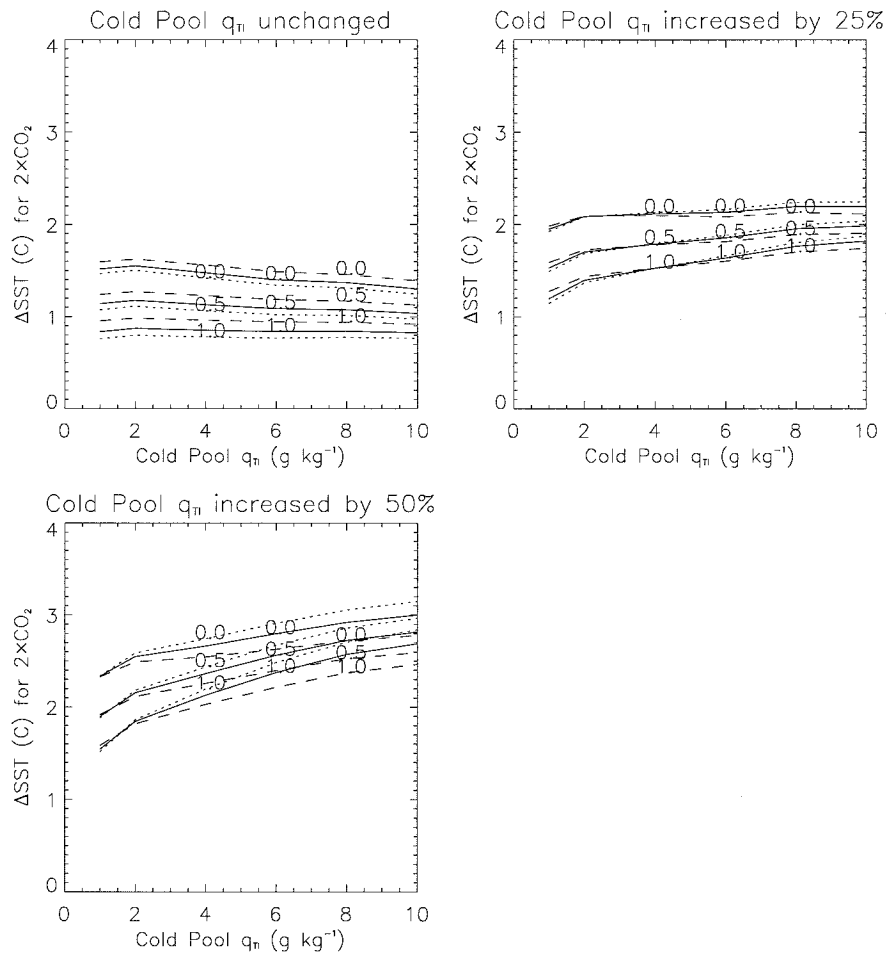


FIG. 12. As in Fig. 7 except that the cloud radiative forcing is calculated using a cloud mixing-line and radiative model, as described in appendix A.

eraged low cloud cover consists of roughly equal parts of cumulus and stratus clouds. We are possibly overestimating the low-cloud forcing since cumulus clouds have optical thicknesses less than 3.6, according to ISCCP, which is far smaller than the value of 9 assumed in our calculation. This is perhaps why the tropical temperatures in Fig. 10a are lower than those computed with the assumption of  $(-15/a_c)$   $\text{W m}^{-2}$  of low-cloud forcing (Fig. 6a). [Clouds in the model of Betts and Ridgway (1989) have comparatively large optical thicknesses of order 100, as estimated from their Fig. 2, resulting in even lower equilibrium temperatures near  $27^\circ\text{C}$ .]

The total cloud optical thickness prior to rescaling—that is, the value that is computed from the cloud liquid water content—is shown in Fig. 11d. The optical thickness is slightly larger than the value of 9 assumed to be consistent with ERBE. We tried to improve the agreement by reducing the cloud thickness by 100 m, but the total optical thickness fell to about 6: nearly a factor of 2, despite only a 20% decrease in cloud thickness. This demonstrates that total cloud optical thickness is very

sensitive to the thickness of the cloud. The reason for this, of course, is that cloud liquid water is generally observed to increase monotonically above cloud base so that deepening of a cloud can significantly increase its total liquid water content and corresponding optical thickness—especially for relatively shallow clouds like marine stratus.

The model's sensitivity to doubled  $\text{CO}_2$  was recalculated using the explicit computation of cloud forcing and the total cloud  $\tau$  set equal to 9. (For this value of  $\tau$ , the sensitivity of TOA cloud forcing to changes in low cloud cover is nearly identical to the empirical value derived by Klein and Hartmann (1955): cf. Fig. 11a.) Perturbations to low cloud cover were computed using (30) as before. The warming for experiments with and without low cloud feedbacks is shown in Fig. 12. The results are virtually identical to those shown in Fig. 7, where cloud forcing independent of height was assumed. This suggests that this idealization does not greatly affect the model sensitivity to climate forcing.

So far, we have ignored the cloud optical thickness feedback, although given our mixing-line parameteriza-

tion of cloud properties, including liquid water, this feedback could be included. For example, we could tune cloud depth in order to result in a value of total cloud optical thickness that is consistent with the ERBE TOA forcing. Then, it would be tempting to allow total cloud optical thickness to vary with the cloud liquid water content as  $\text{CO}_2$  increases so that we could study the importance of low-cloud optical thickness feedbacks in comparison with low cloud cover feedbacks. However, this seems ill-advised given the extreme dependence of the total optical thickness upon cloud thickness. We have no way of estimating how this latter parameter will change with increasing  $\text{CO}_2$ . Furthermore, we might expect the cloud condensation nuclei concentration to change, which would alter the droplet size distribution. This would change the effective droplet radius  $r_e$ , which is important to our calculation of optical thickness. Any optical thickness feedbacks that our model produces would presumably be attended by large uncertainties as a result of these effects.

#### APPENDIX B

##### How Does $T_{s,w} - T_{s,c}$ Change in Response to Doubled $\text{CO}_2$ ?

In section 4, it was shown that stratus low cloud cover depends upon the difference in surface temperature between the warm and the cold pools [cf. (32)]. Furthermore, it was found that this difference, denoted by  $T_{s,w} - T_{s,c}$ , increases in response to doubled  $\text{CO}_2$ . This is a result that is independent of the presence of the low cloud cover feedback (Fig. 7a) and, instead, reflects how our simple model of the tropical circulation responds to increasing  $\text{CO}_2$ . In this appendix, we examine why this increase occurs, while attempting to anticipate whether this increase would occur if certain processes currently held fixed—for example, transport by midlatitude eddies and the ocean circulation, along with changes in cold pool upper-tropospheric moisture—were allowed to respond to changes in the  $\text{CO}_2$  concentration.

Consider first the radiative effect of increasing the  $\text{CO}_2$  concentration. This increases the longwave opacity of the atmospheric column and by itself reduces the OLR. In the absence of horizontal energy redistribution by a large-scale circulation or a reduction in upper tropospheric moisture, equilibrium requires that the temperature of the column increase in order to restore the original value of OLR.

Although  $\text{CO}_2$  is assumed to increase uniformly over the warm and cold pools, the increase in opacity is larger over the warm pool. This is because in our model, upper-tropospheric water vapor increases in response to rising surface temperatures over the warm pool, while the cold pool value is held fixed. (This distinction is based upon the proximity of the warm pool to the deep convective towers that are expected to intensify in response to warming of the surface by increased  $\text{CO}_2$ .) Because of

the large-scale circulation linking the two regions, temperatures are identical above the trade inversion. Thus, the warm pool OLR will increase less than the cold pool value as the concentration of  $\text{CO}_2$  rises, since the opacity of the warm pool column is larger but the temperatures of the two columns are identical. (Beneath the trade inversion, the warm pool temperature can exceed the cold pool value, but we assume that longwave emission to space occurs entirely above this level as a result of the large opacity associated with upper-tropospheric moisture.)

Because transports to the extratropics by midlatitude eddies and the ocean circulation are assumed fixed, the tropically averaged OLR must return to its original value in order to restore equilibrium, despite the increased concentration of  $\text{CO}_2$ . Because the perturbed OLR over the warm pool is smaller than the cold pool value  $R_w(z_T)$ , the *net* radiative forcing of the warm pool column increases, while the cold pool loses radiative energy.

Recall (28), the moist static energy budget of the warm pool:

$$a_w R_w(z_T) = -a_w F_{o,w} + a_c M_c (h_{B,w} - h_{B,c}). \quad (28)$$

If ocean transports are fixed, then the warm pool radiative gain associated with doubled  $\text{CO}_2$  must be balanced by increased export of moist static energy, either through an invigorated Hadley–Walker circulation  $M_c$ , or an increased gradient of moist static energy between the warm and cold pools,  $h_{B,w} - h_{B,c}$ , or both. If we denote the unperturbed climate state with an overbar and the perturbation forced by doubled  $\text{CO}_2$  with a “ $\delta$ ,” then (28) can be written to first order in the perturbed quantities as

$$\frac{\delta(h_{B,w} - h_{B,c})}{\bar{h}_{B,w} - \bar{h}_{B,c}} + \frac{\delta M_c}{\bar{M}_c} = \frac{\delta[R_w(z_T) + F_{o,w}]}{\bar{R}_w(z_T) + \bar{F}_{o,w}}. \quad (35)$$

For simplicity, assume that the mixed-layer relative humidities are equal and unchanged by the increase in  $\text{CO}_2$ . Then we can write  $q_{B,w}$  equal to  $rq^*(T_{s,w})$ , which can be approximated as

$$rq^*(T_0) + r \frac{dq^*}{dT} (T_{s,w} - T_0),$$

where  $r$  is the relative humidity and  $q^*$  is the saturation value of specific humidity. Expanding the cold pool mixed-layer specific humidity similarly, we can write  $h_{B,w} - h_{B,c}$  as  $C_p(1 + \gamma)(T_{s,w} - T_{s,c})$ , where  $\gamma$  equals

$$\frac{Lr}{C_p} \frac{dq^*}{dT}.$$

Then (35) becomes

$$\frac{\delta(T_{B,w} - T_{B,c})}{\bar{T}_{B,w} - \bar{T}_{B,c}} + \frac{\delta M_c}{\bar{M}_c} = \frac{\delta[R_w(z_T) + F_{o,w}]}{\bar{R}_w(z_T) + \bar{F}_{o,w}}. \quad (36)$$

The question is whether the increased radiative flux into the warm pool [ $\delta R_w(z_T) > 0$ ] is balanced by an increased

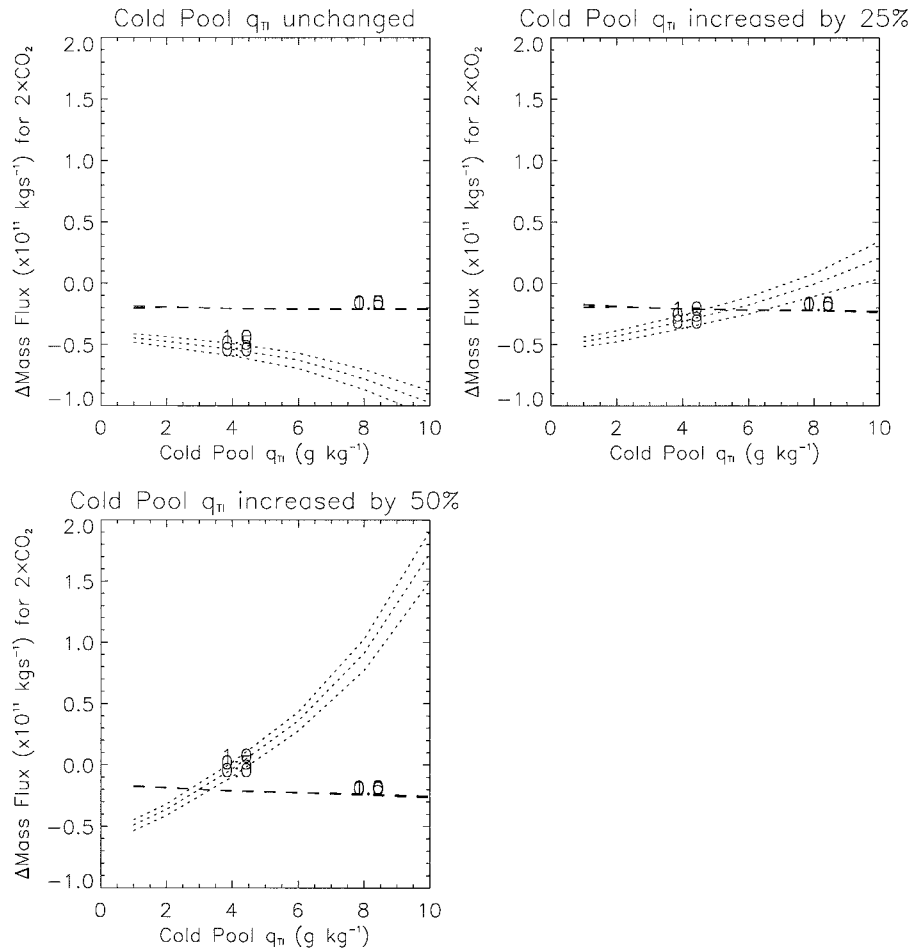


FIG. 13. As in Fig. 7 except for the area-integrated subsidence rate over the cold pool (proportional to  $M_c$ ) and a measure of the strength of the model Hadley–Walker circulation.

circulation, or an increased surface temperature difference, or both.

One might reasonably expect that the large-scale circulation  $\delta M_c$  and the surface temperature difference  $\delta(T_{B,w} - T_{B,c})$  increase together. This is because the mass flux  $a_c M_c$  from the cold pool mixed layer to the warm pool should be in balance with the difference in surface pressure between the two regions. This pressure difference is proportional to the surface temperature difference, based upon the hydrostatic equation (e.g., Schneider 1977; Lindzen and Nigam 1987). Consequently, the radiative gain of the warm pool would be balanced by an increase in both the circulation strength and the surface temperature difference, with the latter leading to an increase in low cloud cover. However, as noted in section 5, this constraint is currently missing from our model, so that the change in  $\delta M_c$  and  $\delta(T_{B,w} - T_{B,c})$  must be inferred by other means.

Combining (26), (4), and (10), we arrive at an equation relating  $M_c$  to  $q_{B,c}$  and various externally prescribed parameters:

$$R_c(z_B) + LF_{m,q} + F_{o,c} = M_c L(q_{B,c} - q_{TL,c}) \quad (37)$$

so that

$$\frac{\delta M_c}{M_c} = -\frac{\delta(q_{B,c} - q_{TL,c})}{\bar{q}_{B,c} - \bar{q}_{TL,c}} + \frac{\delta[R_c(z_B) + LF_{m,q} + F_{o,c}]}{R_c(z_B) + LF_{m,q} + F_{o,c}} \quad (38)$$

The mixed-layer specific humidity will rise with surface temperature in response to increasing  $\text{CO}_2$ . According to (38), this will reduce the magnitude of  $M_c$ . However, the downward flux of radiation at the surface is expected to increase as a result of increased atmospheric absorption and reemission of longwave radiation by  $\text{CO}_2$  so that  $\delta R_c(z_B) > 0$ , and this will tend to increase the circulation. The second effect upon  $M_c$  is comparatively small when  $q_{TL,c}$  is held fixed [ $R_c(z_B)$  is a few  $\text{W m}^{-2}$ ], so that  $M_c$  decreases as the concentration of  $\text{CO}_2$  rises, as shown in Fig. 13.

Because the large-scale circulation weakens in response to increased  $\text{CO}_2$ , the difference in moist static energy and, therefore, surface temperature between the

warm and cold pools must increase in order to export the extra radiation gained by the warm pool. Note that both this difference along with the strength of the circulation depend upon the amount of moisture in the cold pool upper troposphere. The effect of cold pool upper-tropospheric moisture can be seen by comparing Figs. 13a–c. In Fig. 13a,  $q_{\text{TL},c}$  is assumed to be unchanged despite the rising  $\text{CO}_2$  concentration, and  $M_c$  decreases because of the moistening of the mixed layer [cf. Eq. (38)]. In contrast, when  $q_{\text{TL},c}$  is prescribed to increase with  $\text{CO}_2$  as in Figs. 13b,c,  $M_c$  increases for larger values of  $q_{\text{TL},c}$  because the increase in moisture above the trade inversion is greater than the specific humidity increase within the mixed-layer below. The dependence of  $\delta M_c$  upon  $\delta q_{\text{TL},c}$  is reflected in the surface temperature difference. The strengthening of the circulation  $M_c$  with increased cold pool upper-tropospheric moisture allows the warm pool radiative gain to be exported without increasing the surface temperature difference. Note that in Figs. 7b,c,  $(T_{s,w} - T_{s,c})$  decreases when  $q_{\text{TL},c}$  is increased in response to rising  $\text{CO}_2$ , given large enough initial values of  $q_{\text{TL},c}$ . Clearly, the upper-tropospheric moisture feedback within the descending branch of the Hadley–Walker circulation is crucial to the strength of the circulation, the difference in surface temperatures between the warm and cold pools, and thus the low-cloud feedback.

In a simulation of greenhouse warming using a recent version of the GISS atmospheric GCM, the GCM tropical circulation responds to increasing  $\text{CO}_2$  in a slightly different way (A. D. Del Genio 1996, personal communication). The surface temperature difference between the deep Tropics and subtropics is nearly unchanged. Instead, the increased export of moist static energy from the deep Tropics is brought about by an increased gradient of dry static energy at upper levels, which results at least in part from greater warming near the deep tropical tropopause compared to the subtropics. In our simple model, the large-scale circulation is assumed to eliminate this gradient, so that the upper troposphere in the convecting region and subtropics warms identically as the concentration of  $\text{CO}_2$  increases. This is an idealization based upon the behavior of symmetric-circulation models and arguments about angular momentum conservation by the poleward branch of the Hadley circulation in the absence of friction (e.g., Schneider 1977). In the real atmosphere, some friction does exist, although perhaps not as much as is present in the GCM. For now, we simply note that the response of our model to increasing  $\text{CO}_2$  may be sensitive to our assumption of vanishing temperature gradients aloft.

In our simple tropical model, the export of energy to midlatitudes by ocean transports and atmospheric eddies has been held fixed. This export is typically parameterized in terms of the temperature difference between the Tropics and midlatitudes (e.g., Branscome 1983; Nakamura et al. 1994) so that its computation requires knowledge of the midlatitude temperature, which is out-

side of our model domain. Simulations by a coupled ocean–atmosphere GCM suggest that these transports can change (Manabe and Stouffer 1993) as  $\text{CO}_2$  increases, although the total poleward flux of energy remains nearly constant. In particular, ocean transports are found to weaken initially as  $\text{CO}_2$  increases, although they remain at their reduced value only if the  $\text{CO}_2$  concentration is increased by as much as four times the present value. The reduced ocean transports are compensated by increased atmospheric eddy latent heat transports. The effect of changing eddy and ocean transports can be estimated by combining (38) with (36):

$$\frac{\delta(T_{B,w} - T_{B,c})}{\bar{T}_{B,w} - \bar{T}_{B,c}} = \frac{\delta[R_w(z_T) + F_{o,w}]}{\bar{R}_w(z_T) + \bar{F}_{o,w}} + \frac{\delta(q_{B,c} - q_{\text{TL},c})}{\bar{q}_{B,c} - \bar{q}_{\text{TL},c}} - \frac{\delta[R_c(z_B) + LF_{m,q} + F_{o,c}]}{\bar{R}_c(z_B) + \bar{L}\bar{F}_{m,q} + \bar{F}_{o,c}}. \quad (39)$$

The present-day ocean transport  $\bar{F}_{o,c}$  exports heat from the cold pool so that a reduction in transport corresponds to  $\delta F_{o,c} > 0$ . This would reduce the temperature difference implied by (39), although this could be offset by an increase in the latent heat flux ( $\delta LF_{m,q} < 0$ ). Increased export of heat out of the warm pool by equatorial ocean dynamics [ $\delta F_{o,w} < 0$ ], as described by Seager and Murtugudde (1997), would also reduce the temperature difference.

The effect of low clouds upon the temperature difference can be seen using (39). Low clouds reduce the radiation entering the cold pool atmospheric column. As before, we idealize this reduction to be identical at all levels. Then (32) implies

$$\delta R_c(z_T), \delta R_c(z_B) \propto -\delta(T_{s,w} - T_{s,c}) - \delta(\Delta\theta_{w,ma}). \quad (40)$$

The last term increases the right-hand side of (39), while the preceding term reduces the coefficient multiplying  $\delta(T_{s,w} - T_{s,c})$  on the left-hand side of the same equation. (Scale estimates show that this coefficient is reduced but does not change sign, so that all the sensitivities discussed above are not altered by low-cloud feedbacks.) Both of these effects would increase the surface temperature difference.

In summary, the surface temperature difference between the warm and cold pools, which controls stratus cloud cover, increases as  $\text{CO}_2$  rises. This result depends strongly upon the change in cold pool upper-tropospheric moisture, however, which is specified in our model. The result may also depend upon our assumption that temperature gradients above the trade inversion are eliminated by the large-scale circulation. The model also assumes that energy export to the extratropics is unchanged. Our results may be less sensitive to this assumption, according to (39), since CGCM simulations suggest that the total transport out of the Tropics by both the atmosphere and ocean remains nearly constant.

## REFERENCES

- Albrecht, B. A., 1991: Fractional cloudiness and cloud-top entrainment instability. *J. Atmos. Sci.*, **48**, 1519–1525.
- , D. A. Randall, and S. Nicholls, 1988: Observations of marine stratocumulus clouds during FIRE. *Bull. Amer. Meteor. Soc.*, **69**, 618–626.
- , C. S. Bretherton, D. Johnson, W. H. Schubert, and A. S. Frisch, 1995: The Atlantic Stratocumulus Transition Experiment—ASTEX. *Bull. Amer. Meteor. Soc.*, **76**, 889–904.
- Arking, A., 1991: The radiative effect of clouds and their impact on climate. *Bull. Amer. Meteor. Soc.*, **72**, 795–813.
- Augstein, E., H. Schmidt, and F. Ostapoff, 1974: The vertical structure of the atmospheric planetary boundary layer in undisturbed trade winds over the Atlantic Ocean. *Bound.-Layer Meteor.*, **6**, 129–150.
- Bates, J. J., X. Wu, and D. L. Jackson, 1996: Interannual variability of upper-tropospheric water vapor band brightness temperature. *J. Climate*, **9**, 427–438.
- Betts, A. K., 1982: Saturation point analysis of moist convective overturning. *J. Atmos. Sci.*, **39**, 1484–1505.
- , 1990: Greenhouse warming and the tropical water budget. *Bull. Amer. Meteor. Soc.*, **71**, 1464–1465.
- , and B. A. Albrecht, 1987: Conserved variable analysis of boundary layer thermodynamic structure over the tropical oceans. *J. Atmos. Sci.*, **44**, 83–99.
- , and W. Ridgway, 1989: Climatic equilibrium of the atmospheric convective boundary layer over a tropical ocean. *J. Atmos. Sci.*, **46**, 2621–2641.
- Boers, R., and A. K. Betts, 1988: Saturation point structure of marine stratocumulus clouds. *J. Atmos. Sci.*, **45**, 1156–1175.
- Branscome, L. E., 1983: A parameterization of transient eddy heat flux on a beta-plane. *J. Atmos. Sci.*, **40**, 2508–2521.
- Budyko, M. I., and Y. A. Izrael, 1991: Paleoclimatic evidence of climatic sensitivity to changing atmospheric gas concentration. *Anthropogenic Climate Change*, M. I. Budyko and Y. A. Izrael, Eds., University of Arizona Press, 279–318.
- Chou, M.-D., 1994a: Coolness in the tropical Pacific during an El Niño episode. *J. Climate*, **7**, 1684–1692.
- , 1994b: Radiation budgets in the western tropical Pacific. *J. Climate*, **7**, 1958–1971.
- Clement, A. C., R. S. Seager, M. A. Cane, and S. E. Zebiak, 1996: An ocean dynamical thermostat. *J. Climate*, **9**, 2190–2196.
- Deardorff, J. W., 1980: Cloud top entrainment instability. *J. Atmos. Sci.*, **37**, 131–147.
- Del Genio, A. D., and M.-S. Yao, 1993: Efficient cumulus parameterization for long-term climate studies: The GISS scheme. *The Representation of Cumulus Convection in Numerical Models*, *Meteor. Monogr.*, No. 46, Amer. Meteor. Soc., 181–184.
- , W. Kovari, and K. K.-W. Lo, 1996: A prognostic cloud water parameterization for global climate models. *J. Climate*, **9**, 270–304.
- Dijkstra, H. A., and J. D. Neelin, 1995: Ocean–atmosphere interaction and the tropical climatology. Part II: Why the Pacific cold tongue is in the east. *J. Climate*, **8**, 1343–1359.
- Emanuel, K. A., J. D. Neelin, and C. S. Bretherton, 1994: On large-scale circulations in convecting atmospheres. *Quart. J. Roy. Meteor. Soc.*, **120**, 1111–1143.
- Hansen, J., G. Russell, D. Rind, P. Stone, A. Lacis, S. Lebedeff, R. Ruedy, and L. Travis, 1983: Efficient three-dimensional global models for climate studies: Models I and II. *Mon. Wea. Rev.*, **111**, 609–662.
- Hanson, H. P., 1991: Marine stratus climatologies. *Int. J. Climatol.*, **11**, 147–164.
- Hartmann, D. L., and M. L. Michelsen, 1993: Large-scale effects on the regulation of tropical sea surface temperature. *J. Climate*, **6**, 2049–2062.
- , M. E. Oekert-Bell, and M. L. Michelsen, 1992: The effect of cloud type on earth's energy balance: Global analysis. *J. Climate*, **5**, 1281–1304.
- Held, I. M., and A. Y. Hou, 1980: Nonlinearly axially symmetric circulations in a nearly inviscid atmosphere. *J. Atmos. Sci.*, **37**, 515–533.
- Heymsfield, A. J., and L. J. Donner, 1990: A scheme for parameterizing ice–cloud water content in general circulation models. *J. Atmos. Sci.*, **47**, 1865–1877.
- Houze, R. A., and A. K. Betts, 1981: Convection in GATE. *Rev. Geophys. Space Phys.*, **19**, 541–576.
- Kiehl, J. T., 1994: On the observed near cancellation between long-wave and shortwave cloud forcing in tropical regions. *J. Climate*, **7**, 559–565.
- Klein, S. A., and D. L. Hartmann, 1993: The seasonal cycle of low stratiform clouds. *J. Climate*, **6**, 1587–1606.
- , —, and J. R. Norris, 1995: On the relationships among low-cloud structure, sea surface temperature, and atmospheric circulation in the summertime Pacific. *J. Climate*, **8**, 1140–1155.
- Lindzen, R. S., 1990: Some coolness concerning global warming. *Bull. Amer. Meteor. Soc.*, **71**, 288–299.
- , and S. Nigam, 1987: On the role of sea surface temperature gradients in forcing low-level winds and convergence in the Tropics. *J. Atmos. Sci.*, **44**, 2418–2436.
- , A. Y. Hou, and B. F. Farrell, 1982: The role of convective model choice in calculating the climate impact of doubling CO<sub>2</sub>. *J. Atmos. Sci.*, **39**, 1189–1205.
- Manabe, S., and R. T. Wetherald, 1967: Thermal equilibrium of the atmosphere with convective adjustment. *J. Atmos. Sci.*, **24**, 241–259.
- , and R. J. Stouffer, 1993: Century-scale effects of increased atmospheric CO<sub>2</sub> on the ocean–atmosphere system. *Nature*, **364**, 215–218.
- Nakamura, M., P. S. Stone, and J. Marotzke, 1994: Destabilization of the thermohaline circulation by atmospheric eddy transports. *J. Climate*, **7**, 1870–1882.
- Neelin, J. D., and I. M. Held, 1987: Modeling tropical convergence based on the moist static energy budget. *Mon. Wea. Rev.*, **115**, 3–12.
- Norris, J. R., and C. B. Leovy, 1994: Interannual variability in stratiform cloudiness and sea surface temperature. *J. Climate*, **7**, 1915–1925.
- Oreopoulos, L., and R. Davies, 1993: Statistical dependence of the albedo and cloud cover of tropical marine stratocumulus on sea surface temperature. *J. Climate*, **6**, 2434–2447.
- Peixoto, J. P., and A. H. Oort, 1992: *Physics of Climate*. Amer. Inst. Phys., 520 pp.
- Philander, S. G. H., D. Gu, D. Halpern, G. Lambert, N.-C. Lau, T. Li, and R. C. Pacanowski, 1996: Why the ITCZ is mostly north of the equator. *J. Climate*, **9**, 2958–2972.
- Pierrehumbert, R. T., 1995: Thermostats, radiator fins, and the runaway greenhouse. *J. Atmos. Sci.*, **52**, 1784–1806.
- Ramanathan, V., and W. Collins, 1991: Thermodynamic regulation of ocean warming by cirrus clouds deduced from observations of the 1987 El Niño. *Nature*, **351**, 27–32.
- , R. D. Cess, E. F. Harrison, P. Minnis, B. R. Barkstrom, E. Ahmad, and D. L. Hartmann, 1989: Cloud-radiative forcing and climate: Results from the Earth Radiation Budget Experiment. *Science*, **243**, 57–63.
- Randall, D. A., 1980: Conditional instability of the first kind upside-down. *J. Atmos. Sci.*, **37**, 125–130.
- , J. A. Coakley, C. W. Fairall, R. A. Kropfli, and D. H. Lenschow, 1984: Outlook for research on subtropical marine stratiform clouds. *Bull. Amer. Meteor. Soc.*, **65**, 1290–1301.
- Raymond, D. J., 1994: Convective processes and tropical atmospheric circulations. *Quart. J. Roy. Meteor. Soc.*, **120**, 1431–1455.
- Reed, R. J., and E. E. Recker, 1971: Structure and properties of synoptic-scale wave disturbances in the equatorial western Pacific. *J. Atmos. Sci.*, **28**, 1117–1133.
- Riehl, H., 1979: The trade wind inversion. *Climate and Weather of the Tropics*, Academic Press, 202–249.
- , and J. S. Malkus, 1958: On the heat balance of the equatorial trough zone. *Contrib. Atmos. Phys.*, **52**, 503–538.

- Rossow, W. B., and R. A. Schiffer, 1991: ISCCP cloud data products. *Bull. Amer. Meteor. Soc.*, **72**, 2–20.
- , and Y.-C. Zhang, 1995: Calculation of surface and top of atmosphere radiative fluxes from physical quantities based upon ISCCP data sets. 2. Validation and first results. *J. Geophys. Res.*, **100**, 1149–1181.
- Sarachik, E. S., 1974: The tropical mixed layer and cumulus parameterization. *J. Atmos. Sci.*, **31**, 2225–2230.
- , 1978: Tropical sea surface temperature: An interactive one-dimensional atmosphere–ocean model. *Dyn. Atmos. Oceans*, **2**, 455–469.
- Schneider, E. K., 1977: Axially symmetric steady-state models of the basic state for instability and climate studies. Part II: Nonlinear calculations. *J. Atmos. Sci.*, **34**, 280–296.
- Seager, R., and R. Murtugudde, 1997: Ocean dynamics, thermocline adjustment, and regulation of tropical SST. *J. Climate*, **10**, 521–534.
- Slingo, J. M., 1980: A cloud parameterization scheme derived from GATE data for use with a numerical model. *Quart. J. Roy. Meteor. Soc.*, **106**, 747–770.
- , 1987: The development of verification of a cloud prediction scheme for the ECMWF model. *Quart. J. Roy. Meteor. Soc.*, **113**, 899–927.
- Stephens, G. L., 1978: Radiation profiles in extended water clouds. Part II: Parameterization schemes. *J. Atmos. Sci.*, **35**, 2123–2132.
- Sun, D.-Z., and R. S. Lindzen, 1993a: Distribution of tropical tropospheric water vapor. *J. Atmos. Sci.*, **50**, 1643–1660.
- , and —, 1993b: Water vapor feedback and the ice age snow-line record. *Ann. Geophys.*, **11**, 204–215.
- , and A. H. Oort, 1995: Humidity–temperature relationships in the tropical troposphere. *J. Climate*, **8**, 1974–1987.
- , and Z. Liu, 1996: Dynamic ocean–atmosphere coupling: A thermostat for the tropics. *Science*, **272**, 1148–1150.
- Tennekes, H., 1973: A model for the dynamics of the inversion above a convective boundary layer. *J. Atmos. Sci.*, **30**, 558–567.
- Thompson, R. M., S. W. Payne, E. E. Recker, and R. J. Reed, 1979: Structure and properties of synoptic-scale wave disturbances in the intertropical convergence zone of the eastern Atlantic. *J. Atmos. Sci.*, **36**, 53–72.
- Tselioudis, G., W. B. Rossow, and D. Rind, 1992: Global patterns of cloud optical thickness variation with temperature. *J. Climate*, **5**, 1484–1495.
- Wallace, J. M., 1992: Effect of deep convection on the regulation of tropical sea surface temperature. *Nature*, **357**, 230–231.
- Wang, J., and W. B. Rossow, 1995: Determination of cloud vertical structure from upper-air observations. *J. Appl. Meteor.*, **34**, 2243–2258.
- Wang, Q., and B. A. Albrecht, 1994: Observations of cloud-top entrainment in marine stratocumulus clouds. *J. Atmos. Sci.*, **51**, 1530–1547.
- Xu, K.-M., and K. A. Emanuel, 1989: Is the tropical atmosphere conditionally unstable? *Mon. Wea. Rev.*, **117**, 1471–1479.
- Yang, H., and R. T. Pierrehumbert, 1994: Production of dry air by isentropic mixing. *J. Atmos. Sci.*, **51**, 3437–3454.